Journal of
Medicinal Chemistry

Article

Discovery of a Novel Cabazitaxel Nanoparticle-Drug Conjugate (CRLX522) with Improved Pharmacokinetic Properties and Anticancer Effects using a #-Cyclodextrin-PEG Copolymer-Based Delivery Platform

Chester Metcalf, Sonke Svenson, Jungyeon Hwang, Snehlata Tripathi, Geeti Gangal, Sujan Kabir, Douglas Lazarus, Roderic Cole, Beata Sweryda-Krawiec, Pochi Shum, Donna Brown, Roy Case, Derek van der Poll, Ellen Rohde, Stephanie Harlfinger, Chi-Hse Teng, and Scott Eliasof

J. Med. Chem., **Just Accepted Manuscript** • DOI: 10.1021/acs.jmedchem.9b00892 • Publication Date (Web): 08 Oct 2019

Just Accepted

is published by the American Chemical Society. 1155 Sixteenth Street N.W., Washington, DC 20036

Discovery of a Novel Cabazitaxel Nanoparticle-Drug Conjugate (CRLX522) with Improved Pharmacokinetic Properties and Anticancer Effects using a β-Cyclodextrin-PEG Copolymer-Based Delivery Platform

Chester A. Metcalf III*[1], Sonke Svenson[2], Jungyeon Hwang[2], Snehlata Tripathi[2], Geeti Gangal[2], Sujan Kabir[2], Douglas Lazarus[2], Roderic Cole[2], Beata Sweryda-Krawiec[2], Pochi Shum[2], Donna Brown[2], Roy I. Case[1], Derek van der Poll[2], Ellen Rohde[2], Stephanie Harlfinger[1], Chi-Hse Teng[1], Scott Eliasof[2]

[1]Novartis Institutes for BioMedical Research Inc., 181 Mass Ave, Cambridge, MA 02139 USA

[2]Cerulean Pharma Inc., 35 Gatehouse Drive, Waltham, MA 02451 USA

Corresponding author:

*Chester A. Metcalf III, Novartis Institutes for BioMedical Research Inc., 181 Mass Ave, Cambridge, MA 02139 USA; 617-871-7674; chet.metcalf@novartis.com

Abstract

Novel nanoparticle-drug conjugates (NDCs) containing diverse, clinically-relevant anticancer drug payloads (docetaxel, cabazitaxel, and gemcitabine) were successfully generated and tested in drug discovery studies. The NDCs utilized structurally varied linkers that attached the drug payloads to a β-cyclodextrin-PEG copolymer to form self-assembled nanoparticles. *In vitro* release studies revealed a diversity of release rates driven by linker structure-activity relationship (SAR). Improved *in vivo*

pharmacokinetics (PK) for the cabazitaxel (CBTX) NDCs with glycinate- (**1c)** and hexanoate-containing linkers (**2c)** were demonstrated, along with high and sustained tumor levels (>168 hrs of released drug in tumor tissues). This led to potent efficacy and survival in both taxane- and docetaxel-resistant *in vivo* anticancer mouse efficacy models. Overall, the CBTX-hexanoate NDC **2c** (CRLX522) demonstrated an optimal and improved *in vivo* PK (plasma and tumor) and efficacy profile *vs.* parent drug, and the results support the potential therapeutic use of CRLX522 as a new anticancer agent.

1. Introduction

Cancer therapy still remains one of the most challenging treatment areas despite the efforts and progress achieved over the past decade.[1, 2] Poor survival outcomes of current treatments, especially against multi-drug resistant tumors, call for improved therapies with innovative approaches to drug delivery. The treatment of solid tumors with targeted (*e.g.*, tyrosine kinase inhibitors) and cytotoxic drugs face several challenges: (1) Poor drug solubility due to the highly lipophilic nature of many small molecules and/or poor membrane permeability; (2) Poor pharmacokinetic (PK) and absorption, distribution, metabolism, and excretion (ADME) properties of small molecule drugs caused by metabolizable functionality resulting in high clearance rates; (3) Reduced efficacy due to a lack of sustained drug concentrations in tumor tissue as well as non-specific binding to cells and tissues, expressed by large volumes of distribution (V_D); and (4) Toxicity caused by adverse drug effects on healthy tissue. The encapsulation of drug molecules into nanosized carriers has become a powerful approach to address these challenges by increasing solubility, enhancing apparent drug half-life, and targeting tumors and sites of inflammation (*vs.* healthy tissue) via the enhanced permeability and retention (EPR) effect (*i.e.*, accumulation of nanosized molecules and delivery systems selectively to tumor and inflamed tissue via leaky neovasculature coupled with reduced lymphatic drainage).[3-10] The most often studied nanocarriers include liposomes, micelles, and polymeric nanoparticles. A sizable number of nanomedicines based on the three carriers groups have translated into the clinic, and some have advanced to marketed products and are benefiting patients.[11-15] Liposomes and

micelles, albeit important contributors to the field of nanotechnology and nanomedicine, have been extensively described elsewhere[16-25] and therefore the remainder of this section will focus on the properties and characterization of polymeric nanoparticles.

Polymeric nanoparticles are mainly prepared through the use of emulsions or precipitation processes and can involve either physical entrapment of the drug or chemical conjugation (i.e., covalent attachment) between drug and the constituent polymers.[26-30] Nanoparticle sizes depend on the preparation method, ranging from ten to several hundred nm. Nanoparticles requiring a processing step allow engineering of polymeric nanoparticles (size, shape, surface composition, and drug loading efficiency) to be tailored to the respective application needs, but adds to the complexity of manufacturing, particularly at commercial scale.[31-37] Drug encapsulation into polymeric nanoparticles not only improves aqueous solubility, but has the potential for an improved PK profile of the nanoparticle drug (via slow, sustained release) compared to dosing of the drug alone. Such improvements in PK are manifested in increased half-life and AUC in tumors, less frequent dosing (every 2-3 weeks in some cases) and reduced biodistribution into healthy tissue, which can result in lower toxicity.[38-41] In addition, polymeric nanoparticles, with sizes above 10 nm but preferably below 100 nm, can take advantage of selective tumor accumulation via the EPR effect (in addition to low V_D) to improve target specificity of the treatment, and consequently, the efficacy of the respective drug. [42,43] This combination of reduced toxicity and enhanced efficacy has the potential to improve the therapeutic index.[14, 44]

Given the two methods of physical entrapment and chemical conjugation to encapsulate drugs into polymeric nanoparticles, most approaches rely on physical entrapment of the drug. There are two major challenges with this approach: (1) The hydrophilic or hydrophobic (in most cases) nature of the drug has to match that of the polymeric carrier to achieve sufficiently high drug loading; and (2) Release of physically entrapped drugs generally shows bi-phasic behavior where an initial burst release of the drug is followed by first-order sustained release.[45-47] This bi-phasic behavior is a more than likely a consequence of drug molecules on or close to the polymeric nanosurface that are released instantaneously under the sink

condition of the bloodstream, along with other complexities of the drug-loaded nanoparticle system. Reducing burst release and improving entrapment efficiency to provide sustained release of drug and potentially greater efficacy often require more complex formulation approaches.[48, 49] Chemical drug conjugation on the other hand has several advantages over physical entrapment: (1) The initial burst release of drugs can be greatly reduced or avoided; (2) Conjugation can protect small molecule drugs from being metabolized until after the payload is released from the nanoparticle carrier, leading to sustained release of intact drug; (3) Linker molecules between drug and carrier can be designed to release drugs with varying and differentiating *in vivo* kinetics in response to a trigger event (*e.g.*, changes in pH, temperature, or enzyme levels), allowing much greater control over drug release compared to diffusion and matrix degradation; and (4) Conjugation of drugs to the constituent polymers allows nanoparticle formation regardless of the drugs' physicochemical characteristics (*e.g.*, hydrophobicity).[50-54] Drug encapsulation through chemical conjugation linker strategies to form nanoparticle-drug conjugates (NDCs), using a β-cyclodextrin-PEG (CDP) copolymer, has been the focus of our current efforts (*vide infra*) to deliver therapeutic levels of released small molecule drug payloads to the tumor microenvironment, reduce systemic drug levels (*i.e.*, increase therapeutic indexes - TIs), and provide effective treatments for solid tumor indications.[39-41] The first clinical compound (CRLX101) to evolve from the NDC platform advanced to Phase 2 clinical development.[40, 55] CRLX101 contains camptothecin (CPT) as the payload and glycine as the linker molecule. The second clinical compound CRLX301 (compound **5c**), containing docetaxel as the payload and glycine as the linker molecule, completed Phase 1 clinical development.

Herein we present results that demonstrate the ability to modulate PK parameters and provide sustained and controlled release kinetics for novel NDCs containing the active pharmaceutical ingredient (API) drug payloads docetaxel (DTX), cabazitaxel (CBTX), or gemcitabine (GEM) using a proprietary linker technology platform. From a PK perspective, we are aiming to increase the apparent half-life of the drug as well as reduce plasma C_{max} by making the release rate of the drug payload from the NDC the rate-limiting step. The polymeric backbone of the nanoparticles employed in this study utilizes the CDP copolymer

technology. A series of *in vivo* PK and efficacy studies were conducted in tumor-bearing mice to establish *in vitro* to *in vivo* structure-activity relationship (SAR) correlations. This resulted in the discovery of CBTX-hexanoate NDC **2c** (CRLX522), which has potential therapeutic use as a new anticancer agent.

2. Results and Discussion

2.1. Synthesis and Formation of Nanoparticle Drug Conjugates (NDCs)

The syntheses of CBTX, DTX, and GEM NDCs are shown in Schemes 1-3. Drug loading for CBTX **1c-4c** and DTX **5c-8c** NDCs was high (71-100%) and approaching or at theoretical values, whereas loading for the GEM NDCs **11c-13c** was at about half the theoretical values (Table 1); such lower loaded NDCs, which leave uncapped negatively charged carboxylic acid groups that have relatively fewer number of stabilizing cyclodextrin-API inclusion complexes within the NDC, have been shown previously to result in higher AUC of *in vivo* released drug.[41] Nonetheless, all NDCs self-assembled in water to form nanoparticles between 17-28 nm in average size (Zavg) as measured by dynamic light scattering (DLS). An exception were the nanoparticles formed by the CBTX-disulfide-carbonate NDC **4c**, which gave a Zavg value of 194 nm. This larger particle size, which was only observed for the CBTX-disulfide NDC **4c**, could be an indication of crosslinking between copolymer strands caused by the reversible nature of the disulfide bond. Similar issues were observed with the GEM disufide linker and attempts to synthesize the NDC in high purity were unsuccessful. This led to the conclusion that GEM was not a good synthetic candidate for the disulfide linker conjugation. Due to crosslinking potentially complicating interpretation of release kinetics as well as the larger particle size of the CBTX-disulfide NDC not allowing direct comparison to the other smaller nanoparticles, NDC **4c** was not tested in subsequent studies. Unexpectedly, these issues were not observed for the closely related taxane NDC, DTX disulfide analogue **8c**. The polydispersity indices (PDIs) of all self-organized structures were sufficiently narrow with values between 0.2 and 0.5, and the aqueous NDC solutions all had high drug purities (>95% for all tested NDCs) and high drug concentrations (1.2-4.5

mg/mL). We have previously reported successful generation of cryo-TEM images of NDC nanoparticles (e.g., CRLX101).[41]

Table 1. Characterization, concentration, loading, and purity data for CBTX, DTX, and GEM NDCs.

Drug-linker NDCs	Zavg[a] (nm)	PDI	NDC Drug Conc[b] (aq., mg/mL)	Theoretical Drug Loading (weight %)	Actual Drug Loading[b] (weight %)/% of Theoretical	NDC Drug Purity[b] (%)
CBTX-glycinate NDC (1c)	24.8	0.231	3.4	25.4	20.4/80	99
CBTX-hexanoate NDC (2c)	27.8	0.249	3.1	25.0	17.7/71	99
CBTX-alaninate NDC (3c)	22.7	0.251	3.3	25.3	19.1/75	100
CBTX-disulfide-carbonate NDC (4c)	194	0.313	4.3	24.5	19.3/79	91
DTX-glycinate NDC (5c)	26.1	0.286	3.5	24.8	22.4/90	98
DTX-hexanoate NDC (6c)	18.4	0.367	1.7	24.3	16.9/70	97
DTX-β-alanine-glycolate NDC (7c)	24.7	0.214	4.5	24.2	18.0/74	95
DTX-disulfide-carbonate NDC (8c)	26.4	0.487	3.6	23.9	23.9/100	98
GEM-glycinate NDC (11c)	27.4	0.223	1.2	8.29	3.8/46	100
GEM-hexanoate NDC (12c)	17.0	0.269	2.1	8.13	4.3/53	100
GEM-β-alanine-glycolate NDC (13c)	18.5	0.194	3.4	8.08	4.2/52	98

[a] Size measured by dynamic light scattering (DLS). [b] Drug concentration, loading and purity measured by reverse phase (RP) high-pressure liquid chromatography (HPLC).

Scheme 1. Synthesis of cabazitaxel-linkers

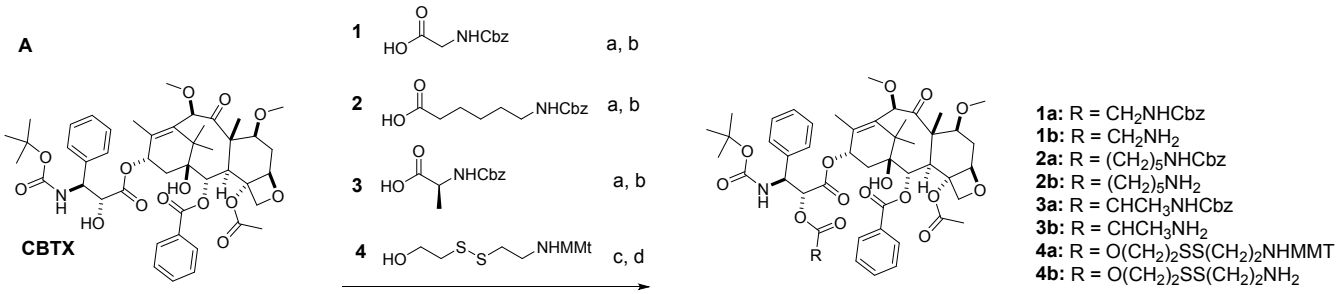

Reaction conditions: (a) *N*-Cbz amino acid (**1-3**), EDC, DMAP; (b) H_2, Pd/C, MsOH; (c) **4**, *N*-hydroxysuccinimide carbonate, DMAP; (d) Dichloroacetic acid, anisole.

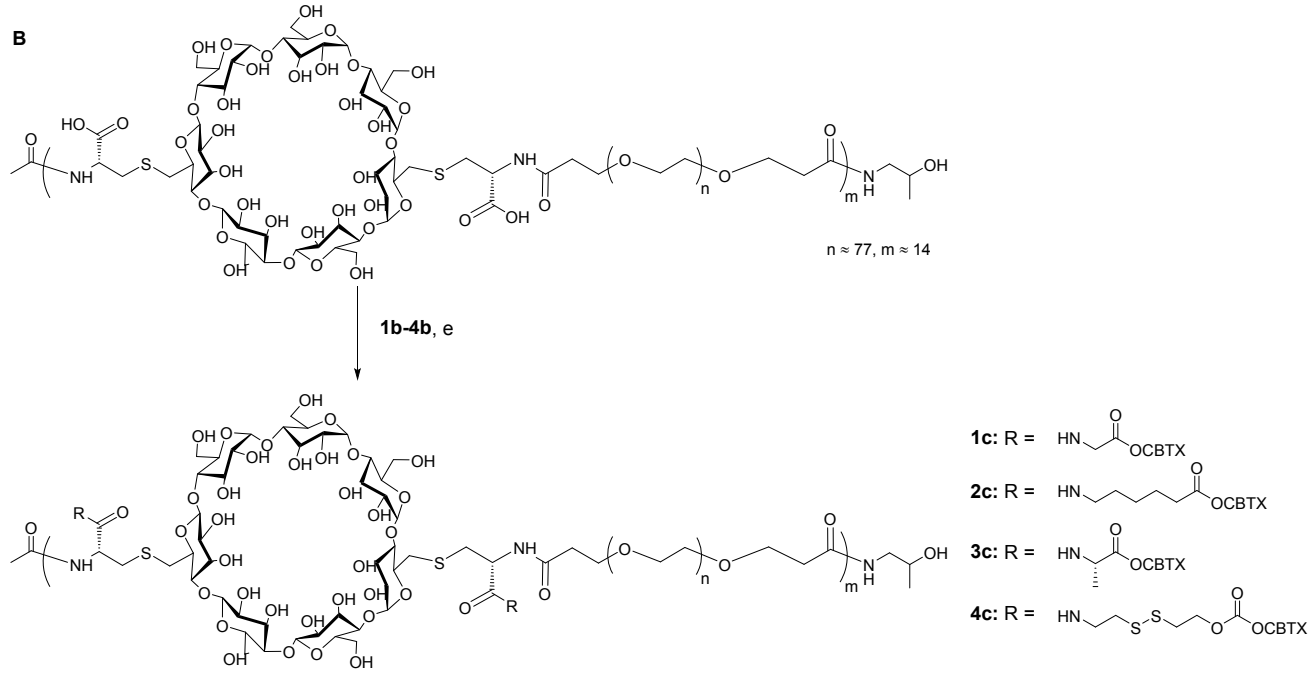

Reaction conditions: (e) EDC, NHS, (**1b-4b**).

Scheme 1. Syntheses of CBTX NDCs **1c-4c**. (A) Reaction of CBTX with linkers. (B) Conjugation of CBTX-linker molecules to the CDP copolymer to give the corresponding CBTX NDCs following purification/processing.

Scheme 2. Synthesis of docetaxel-linkers

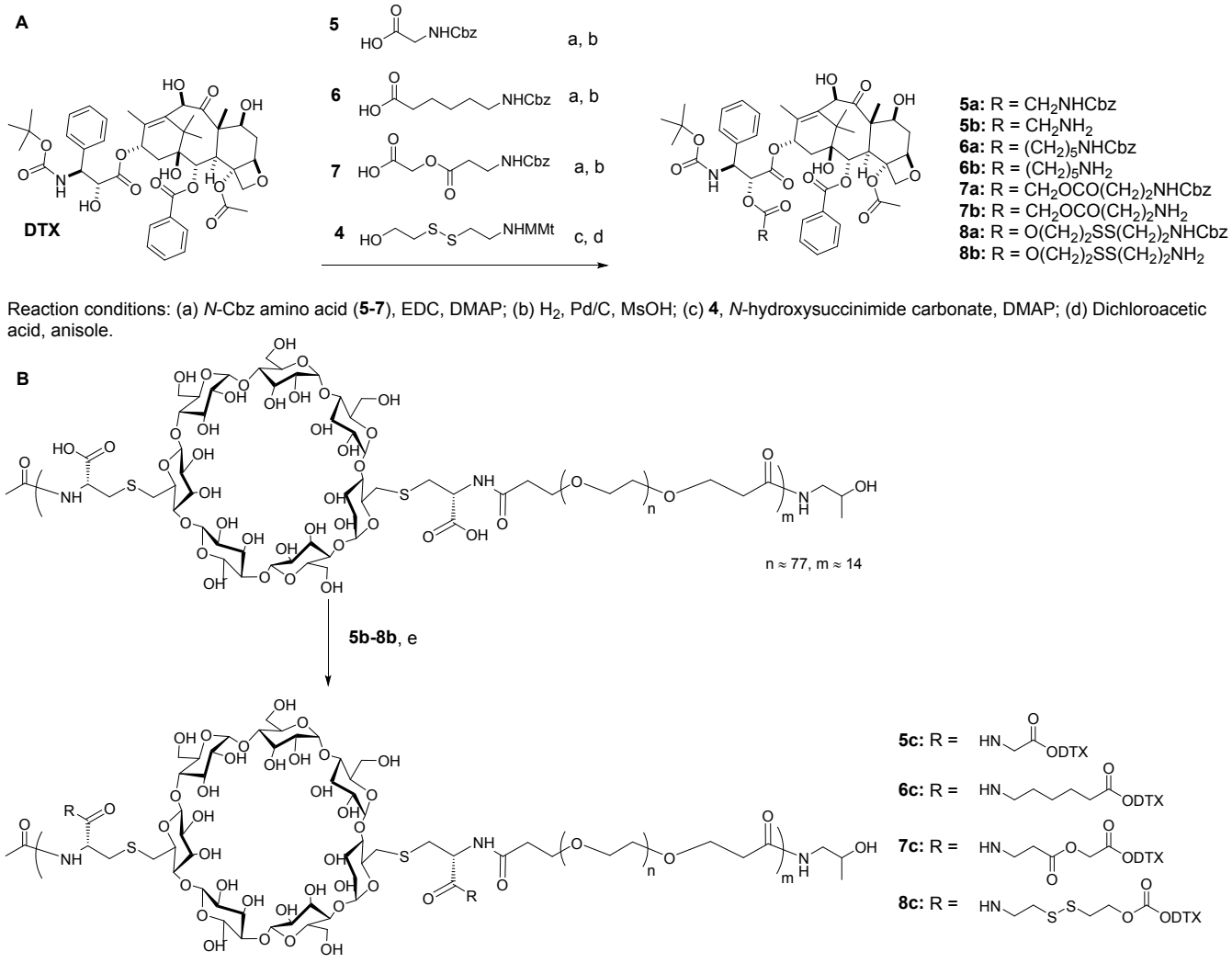

Scheme 2. Synthesis of DTX NDCs **5c-8c**. (A) Reaction of DTX with linkers. (B) Conjugation of DTX-linkers to CDP copolymer to give the corresponding DTX NDCs following purification/processing.

Scheme 3. Synthesis of gemcitabine-linkers

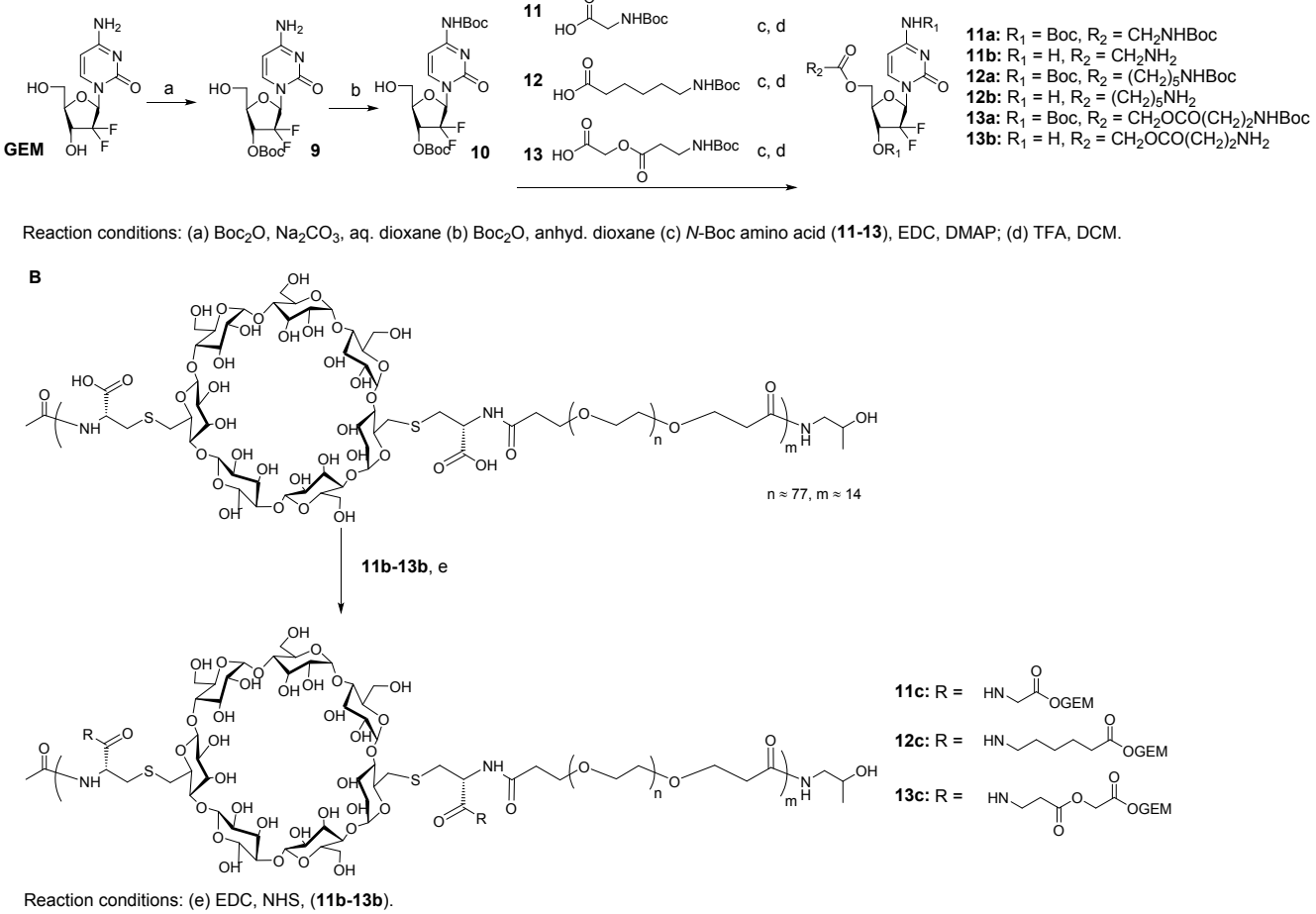

Scheme 3. Syntheses of GEM NDCs **11c-13c**. (A) Reaction of GEM with linkers. (B) Conjugation of GEM-linkers to the CDP copolymer to give the corresponding GEM NDCs following purification/processing.

2.2. In vitro Release of Docetaxel, Cabazitaxel, and Gemcitabine NDCs

The *in vitro* rates of drug release from DTX-, CBTX- and GEM-containing NDCs using a variety of different linkers under near physiological conditions (*i.e.*, phosphate-buffered saline (PBS) at pH 7.4 and 37 ^{o}C) were investigated to demonstrate the influence of linker functionality on drug release kinetics. The three drugs were conjugated to 5 possible linker molecules (glycinate, alaninate, hexanoate, diester β-alanine-glycolate, and disulfide-carbonate) with varying degrees of hydrophobicity, length, and ester functionality/sterics/electronics. Matched sets of linker NDCs (i.e., only API drug payload varied) were

generated for the purpose of comparing linker release trends between structurally similar (CBTX, DTX) and dissimilar (GEM) drugs. Glycinate, alaninate, and hexanoate linkers were chosen to determine the effects of varied linker hydrophobicity, sterics and electronics (e.g., α-amino acid *vs.* aliphatic ester) on release kinetics, and all utilized hydrolysis sensitive ester bonds to attach their respective drugs. In addition, two linkers with dual sites for drug release were studied: a β-alanine-glycolate containing-linker with two hydrolysable ester bonds, and a disulfide-carbonate linker with potential for additional intracellular glutathione (GSH) triggered release.[56]

The *in vitro* release profiles of DTX NDCs **5c-8c** with the various linker molecules are shown in Fig. 1. The bis ester-containing β-alanine-glycolate (β-Ala-glyc) linker showed the fastest release, potentially due to the dual release mechanism and/or increased hydrolytic lability of the API-linked ester bond (driven by adjacent electron-withdrawing group), with ~90% of DTX released by 24 hr. The glycinate linker released 50-60% DTX within that time period, while the longer and more hydrophobic hexanoate linker and the disulfide-carbonate linker both released less than 15% DTX by 72 hrs. The slower release for the **6c** and **8c** linkers can be rationalized by the more hydrophobic and/or presumed less hydrolytically labile ester linker functionality, leading to reduced chemical hydrolysis in the hydrophobic nanoparticle core and a more stabilized NDC. The observed plateau around 60% release of DTX from the glycinate NDC is due to the formation of 7-epidocetaxel (data not shown), and appears to be specific to the DTX payload-glycinate linker combination.

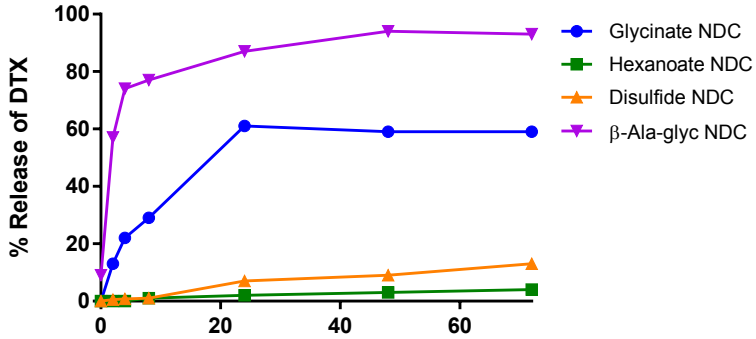

Figure 1. *In vitro* release of DTX from DTX NDCs **5c-8c** in PBS at pH 7.4 and 37°C.

The release profile trends for the CBTX NDCs **1c-4c** were similar to DTX NDCs, with the faster release rate observed for the glycinate linker (>90% by 72 hr) and slower release measured for the hexanoate linker (<5% by 72 hrs) as shown in Fig. 2A. Both CBTX NDC linkers show a large difference in release % at the initial time points as well (<1 *vs.* ~20%). The alaninate and glycinate linkers showed similar release rates, which suggest that their release is driven by similar electronic factors associated with the common α-amino acid ester linker functionality *vs.* hydrophobicity and/or steric effects. The glycinate and hexanoate linkers (fast and slow release, respectively) were chosen to examine release kinetics in the presence of plasma enzymes to determine the extent by which they contribute to the mechanism of drug release from the NDCs. The CBTX-glycinate **1c** and CBTX-hexanoate **2c** NDCs were mixed with untreated mouse plasma as well as plasma that had been heat-treated to inactivate enzymes. The glycinate conjugate showed somewhat faster release in mouse plasma than PBS (100 *vs*. ~70% by 24 hr), but no release rate differences were observed for untreated *vs.* heat-inactivated plasma (Fig. 2B). The same was true for the hexanoate linker, in which the release rates in PBS, active plasma, and heat-inactivated plasma were essentially identical (Fig. 2C). The faster release of the glycinate linker in plasma *vs.* PBS may be related to the presence of lipoprotein complexes that can assist in the disassembly of the NDC.[41] The more stabilized, hydrophobic hexanoate linker may be less sensitive to these effects leading to the similar release rates in plasma and PBS. Taken together, the *in vitro* release data suggest that plasma enzymes should not play a major role in drug release *in vivo*, and it is likely to be a pH-driven release mechanism. This is consistent with previous data for NDCs with ester-containing linkers (*e.g.*, established pH range dependency on hydrolysis rate, IC_{50} shifts in MTT assays [nontoxic] potentially influenced by cell/endosomal pH effects on release rate).[39] A pH-driven mechanism would be predicted to have an advantage over enzyme-mediated cleavage from a PK translatability/variability standpoint, since there is little dependence on individual factors affecting release (*e.g.*, species-to-species and patient-to-patient plasma/tumor enzyme level differences). In support of this,

previous NDCs (e.g., CRLX101) have translated well from animals to humans and demonstrated low patient-to-patient PK variability in the clinic.[41]

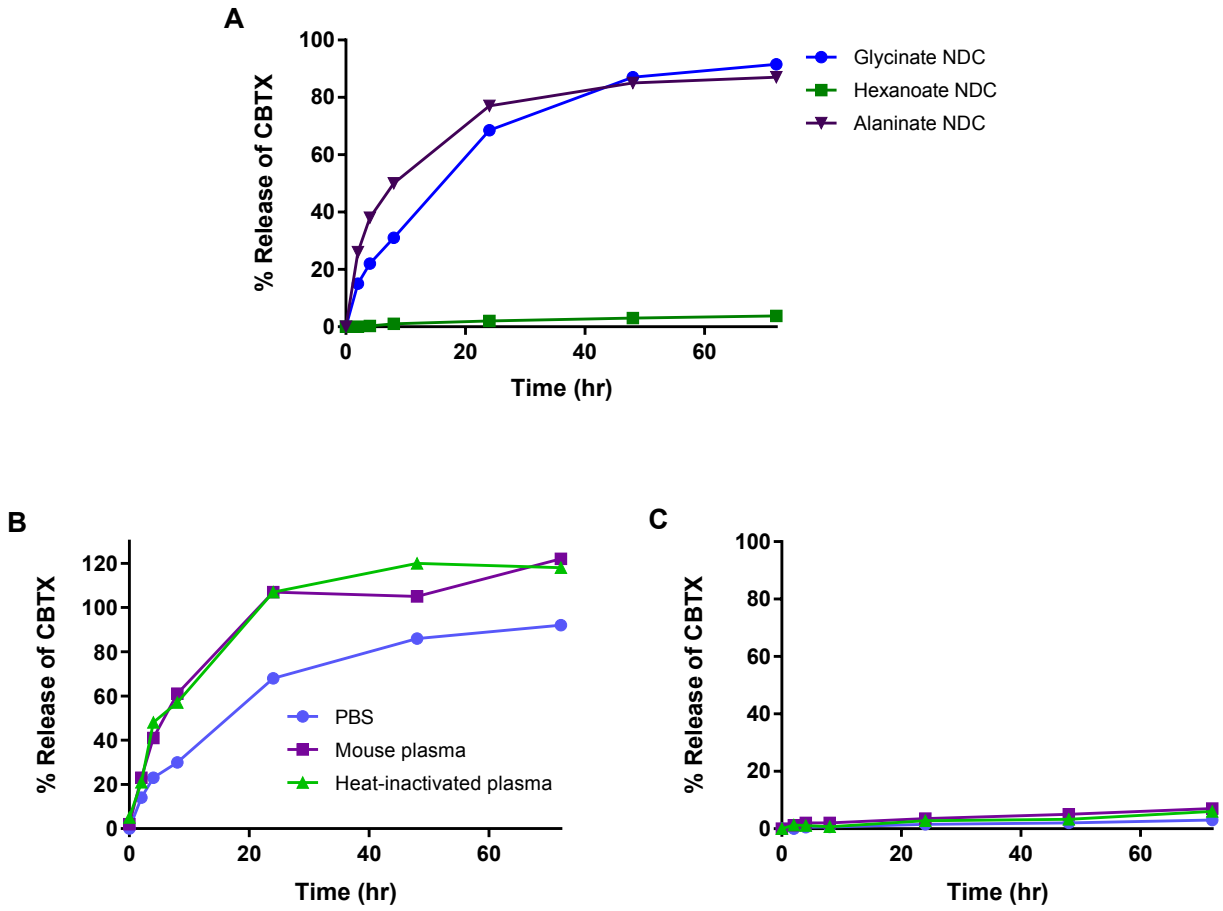

Figure 2. (A) *In vitro* release of CBTX from CBTX NDCs **1c-3c** in PBS at pH 7.4 and 37°C. (B) CBTX-glycinate **1c** and (C) CBTX-hexanoate **2c** NDCs treated with *ex vitro* mouse plasma and heat-inactivated mouse plasma compared to PBS at 37°C.

The release trends for the GEM NDCs **11c-13c** showed some similarities to the DTX and CBTX nanoparticle conjugates (Fig. 3). The β-alanine-glycolate with its two ester groups released drug the fastest (~90% by 24 hr), followed by the glycinate monoester (~60% by 24 hr) and the established slow releasing hexanoate linker (10-15% by 72 hr). It is possible that the faster releasing β-alanine-glycolate and glycinate linkers release drug too fast under the *in vitro* conditions to be differentiated. The collective release data

demonstrate that a range of API payload MW (263-836), lipophilicity (cLogP = -1.5 to 4), and aqueous solubility (1 µM to 100 mM; CBTX and GEM·HCL, respectively) can be accommodated and successfully conjugated into the NDCs while providing sustained and tunable release kinetics. It is conceivable that linker functionality as well as API local structural environment (*e.g.*, primary *vs.* secondary hydroxyl groups) may contribute to overall *in vitro* drug release kinetics. Given the chemical simplicity and the differentiated release profiles for the glycinate and hexanoate linkers, both were selected for further *in vivo* PK studies to establish *in vitro* to *in vivo* SAR correlations for the corresponding NDCs.

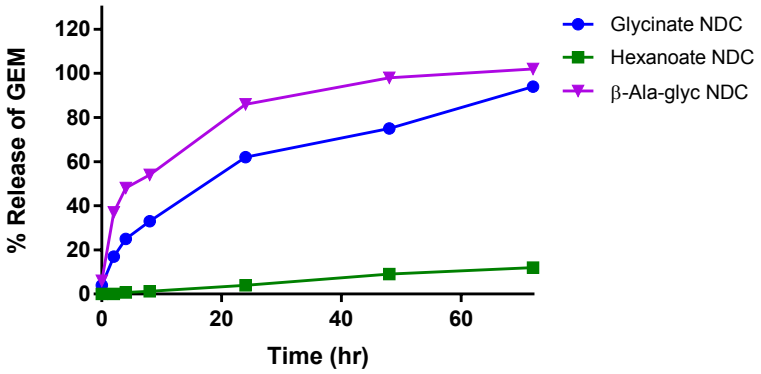

Figure 3. *In vitro* release of GEM from GEM NDCs **11c-13c** in PBS at pH 7.4 and 37°C.

2.3. PK Studies of Cabazitaxel and Gemcitabine NDCs with Glycinate and Hexanoate Linkers

To demonstrate *in vivo* profiles for NDCs with varying release rates, CBTX and GEM payloads were selected for the PK studies. As discussed in the previous section, the two linkers chosen for each API payload were the glycinate linker for fast release and the hexanoate linker for slow release. The corresponding NDC linker pairs for CBTX and GEM were similar in size (hexanoate - 28/glycinate - 25 nm and hexanoate - 17/glycinate - 27 nm, respectively).

In the first study, male C57BL/6 mice with syngeneic B16.F10 tumors[57] were given a single intravenous (iv) doses of CBTX and the respective CBTX NDCs at an equivalent dose of 13.5 mg/kg of CBTX,

providing dose-matched PK and allowing direct comparison of the NDC and parent drug PK data. Animals were sacrificed at different time-points, and plasma and tumor tissue samples were collected for the analysis of total (conjugated + released) drug and released drug levels in each by liquid chromatography with tandem mass spectrometry (LC-MS/MS). The innate ability to hydrolyze the covalent bonds between API and polymer backbone allows for the bioanalytical characterization of the total amount of payload present as well as the quantitation of the released payload from aliquots of the same sample. In plasma, total drug levels approximate conjugated drug levels (calculated by subtracting measured released drug levels from total) due to the much lower released drug levels compared to total (~1% or less of total AUC). The capability to accurately and reliably measure both total and released drug is a key distinguishing feature of the NDC technology, something that is important in a clinical setting and something that is very challenging to accomplish with entrapped polymeric nanoparticles (non-conjugated drug) or liposomes.[41]

Table 2. Plasma PK parameters after a single iv dose of 13.5 mg/kg CBTX, CBTX-glycinate NDC **1c** or CBTX-hexanoate NDC **2c** was given to male C57BL/6 mice with B16.F10 syngeneic tumors.

Test Article		**AUC_∞** [μM*h]	**C_0** or **C_{max}** [μM]	**t_{max}** [hr]	**Cl** [mL/min/kg]	**$t_{1/2}$** [h]	**V_D**[a] [L/kg]	**F**[b] [%]
CBTX		8.4	10	-	32	48	84	-
CBTX-glycinate NDC **1c**	Total	1713	254	-	0.16	23	0.11	-
	Released	20	2.7	0.5	-	14	-	240
CBTX-hexanoate NDC **2c**	Total	7700	382	-	0.035	31	0.09	-
	Released	15	0.22	0.08	-	180	-	178

[a] V_D is calculated as V_{ss} (estimated volume of distribution at steady state) for nanoparticles dosed iv. [b]F = availability of administered CBTX dose in systemic circulation.

Table 3 Tumor PK parameters after a single iv dose of 13.5 mg/kg CBTX, CBTX-glycinate NDC **1c** or CBTX-hexanoate NDC **2c** was given to male C57BL/6 mice with B16.F10 syngeneic tumors.

Test Article		**AUC_{∞}** [μM*h]	**C_{max}** [μM]	**t_{max}** [hr]	**$t_{1/2}$** [h]	Tumor-to-Plasma AUC Ratio
CBTX		177	3.7	6	31	21:1
CBTX-glycinate NDC **1c**	Total	1375	24	2	64	0.8:1
	Released	407	6.3	6	44	20:1
CBTX-hexanoate NDC **2c**	Total	5454	72	24	59	0.7:1
	Released	606	1.4	24	342	40:1

The levels of total drug in plasma for both the CBTX-glycinate **1c** and CBTX-hexanoate **2c** NDCs were substantially higher than the plasma levels of separately dosed CBTX parent drug at all time points over the 168-hour time period studied (Fig. 4A). The total drug AUCs in plasma were ~200-900 fold higher than that of parent drug (Table 2), and large reductions in steady state volume of distribution for the NDCs (~800-900x) compared to parent were also demonstrated. Similar AUC increases for the NDCs were observed for total drug in tumor tissues (Fig. 4C, Table 3). The total drug AUCs for both the CBTX-glycinate **1c** and CBTX-hexanoate **2c** NDCs in tumor were ~8-30 fold higher, respectively, than parent drug and remained high over the course of the study. The phenomena are a direct consequence of the very low clearance (0.035-0.16 *vs.* 32 mL/min/kg for parent) of the NDCs providing long and high drug level blood circulation times, which have been shown previously to lead to NDC accumulation in and penetration through the tumor.[41] In both plasma and tumor tissue, the CBTX-hexanoate nanoparticles provided higher stability (i.e., slower release) and slower decline of total drug levels compared to the CBTX-glycinate nanoparticles, as demonstrated by ~4-fold higher AUC and lower Cl. This ~4-fold difference in AUC/Cl of

total drug between the glycinate and hexanoate linkers, driven by the differentiated release rates of the linkers, provides predictable *in vitro* to *in vivo* correlation (IVIVC) on a "rank-order" level, and supports the notion that release rates are tunable based on linker design.

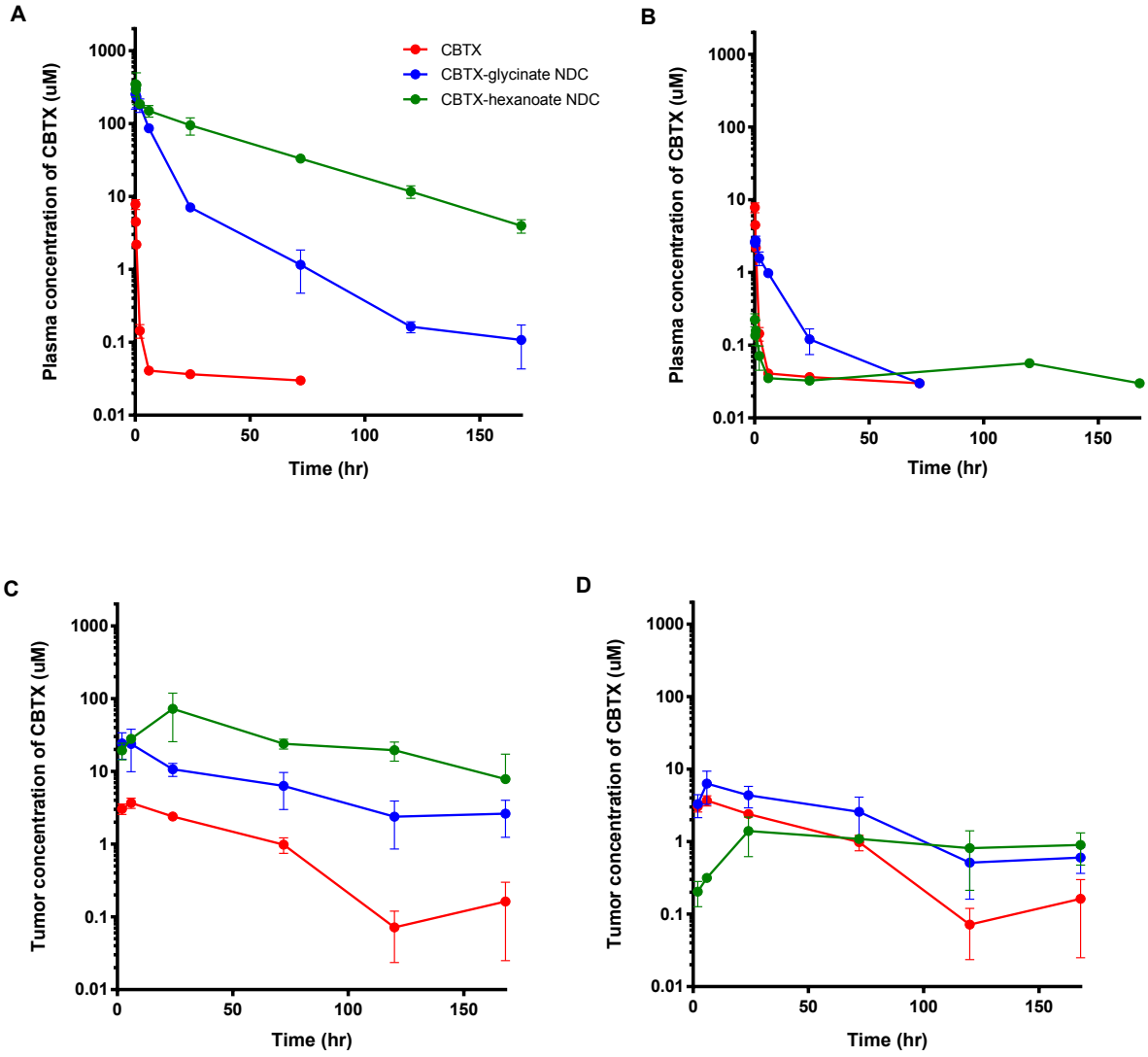

Figure 4. *In vivo* plasma and tumor exposure profiles after separate doses of CBTX, CBTX-glycinate NDC **1c** and CBTX-hexanoate NDC **2c** of 13.5mg/kg each administered iv to male C57BL6/6 mice with syngeneic B16.F10 tumors. (A) Graph for total CBTX in plasma; (B) Graph for released CBTX in plasma; (C) Graph for total CBTX in tumor tissue; (D) Graph for released CBTX in tumor tissue.

The released drug levels for the CBTX-glycinate **1c** and CBTX-hexanoate **2c** NDCs further illustrate the contribution that the linker plays in affecting PK, particularly in plasma (Fig. 4B, Table 2). The differences in released drug AUCs *vs.* parent in plasma are not significant (~2-fold; F ~100%), supportive that Cl of the API is not affected by CBTX NDC administration. However, the PK profiles (e.g., C_{max}, $t_{1/2}$) are quite unique and differentiated between the CBTX-glycinate **1c** and -hexanoate **2c** NDCs as well as separately dosed CBTX parent drug, highlighting the specificity of the drug-linker combination. This differentiated PK is a direct result of the interplay between the varying, rate-limiting *in vitro* release rates for each NDC and *in vivo* PK factors (clearance, plasma protein binding, distribution, etc.), all in dynamic equilibrium, which can have profound effects on the *in vivo* levels of released drug from each NDC; total drug levels are much less influenced by such PK factors as shown previously.[41] Initially, starting concentrations of CBTX in plasma released from the CBTX-glycinate NDC **1c** were ~4-fold lower than for CBTX parent drug, but subsequent time points indicated higher levels of released drug over the course of the study. The initial plasma levels for CBTX released from the CBTX-hexanoate NDC **2c** were ~50-fold lower than parent drug and over 10-fold less than that for CBTX-glycinate NDC **1c**. Although the calculated terminal half-life for released drug from CBTX-hexanoate NDC **2c** is longer than the observation period, it still allows the tentative interpretation that terminal half-life compared to parent drug is increased (~ 4-fold).

PK modulations for the hexanoate linker result in a very flat and sustained released drug PK profile in plasma. The lower C_{max} for both NDCs provides the potential for reduced C_{max}-related toxicities compared to parent drug, while providing sustained levels of released drug over the 168 hour dosing period. The availability of CBTX in systemic circulation after NDC dosing is high (F = ~100-200%), which indicates total conversion assuming Cl of the API is not impaired. By avoiding the initial high C_{max}, optimal NDC selection according to PK/linker release profile is possible to stay below toxic and above efficacious concentrations. The lower released drug plasma PK levels (e.g., C_{max}) for the CBTX-hexanoate NDC **2c** compared to the glycinate NDC **1c**, again controlled by linker design, indicate that the hexanoate NDC

releases drug slower *in vivo* than the glycinate conjugate, and therefore the intact CBTX-hexanoate nanoparticles stay in systemic circulation longer. Longer NDC blood circulation times have the advantage of providing more total drug to the tumor microenvironment, creating a local tumor depot from which sustained levels of drug can be released.

In tumor tissue, the high and sustained levels of released CBTX from both the CBTX-glycinate **1c** and CBTX-hexanoate **2c** NDCs highlight the strengths of the NDC drug delivery platform to provide long-lasting, efficacious levels of drug to the tumor (Fig. 4D, Table 3). The tumor levels of released CBTX from the CBTX-glycinate NDC **1c** provided an exposure profile that was consistently above but similarly shaped to that of CBTX. Released drug tumor levels for the CBTX-hexanoate NDC **2c** were initially low, however, over the course of the 168-hr study the levels of released CBTX from the NDC surpassed those for parent drug (3-4x AUC). Increases in released drug tumor half-life for the CBTX-hexanoate NDC **2c** were realized over both parent drug (>10x) and glycinate NDC **1c** (~8x). Both the CBTX-hexanoate **2c** and CBTX-glycinate **1c** NDCs provided high released drug tumor levels as a percentage of total tumor AUC levels (11% and 30%, respectively). The CBTX-hexanoate NDC **2c** also had high (relative to parent) percent injected dose (ID) delivered into the tumor (1.1%ID), which exceeds the average of 0.7% reported for nanoparticle tumor delivery efficiencies in a survey of 232 data sets.[58] In contrast, only 0.04% of the administered amount of CBTX parent drug reached the tumor. CBTX-hexanoate NDC **2c** also demonstrated an impressive released drug tumor-to-plasma AUC ratio of 40:1, demonstrating differentiation and advantages for the NDC technology over other delivery technologies.[59] Based on overall differentiated and improved PK profiles for the CBTX NDCs, we chose to further explore both in efficacy models as representative of the NDC technology.

The exposure profiles of the GEM-glycinate **11c** and GEM-hexanoate **12c** NDCs were determined in a similar fashion to the previous study by measuring the plasma concentrations of total and released GEM. For the GEM NDCs, our focus was to demonstrate the ability to modulate PK parameters *vs.* parent drug. Therefore, studies were performed in non-tumor bearing mice, which would also allow comparisons

between the CBTX and GEM NDCs given the expectation that plasma PK would be similar in tumor- and non-tumor bearing mice. Non-tumor bearing male C57BL/6 mice were given a single iv dose of the respective GEM NDCs at an equivalent dose of 10 mg/kg GEM, and plasma levels of total and released GEM were measured at several time-points as indicated in Figure 5. The GEM parent drug cleared rapidly from plasma by 3 orders of magnitude within about 12 hours, which is consistent with known extensive deamination of the drug yielding an inactive metabolite. The clinical dosing regimen for the current marketed product recommends high dose weekly administration of 1000 to 1250 mg/m^2 by 30-min iv infusion to achieve therapeutic drug levels and to maximize formation of the active metabolite gemcitabine triphosphate.[60] Encapsulation of GEM into the NDC could shield it from rapid deamination, and slow release of GEM from the NDC form the basis for low continuous exposure levels of the cytotoxic agent. Thus, GEM NDCs may allow for an alternative, improved clinical dosing regimen with fewer toxicities in the clinic.

Except for the initial time-points for released drug, the levels of total and released GEM from both conjugates were higher than GEM parent drug and remained high over 72 hrs (Fig. 5). Both GEM NDCs demonstrated much reduced V_D values (0.02-0.05 L/kg) and clearance (0.037-0.087 mL/min/kg) for total drug compared to parent (1.5 L/kg and 55 mL/min/kg, respectively), in addition to providing increases in total drug plasma half-life (8-12x) as indicated in Table 4. Like the CBTX NDCs, the lower C_{max} of released drug in plasma for the GEM NDCs (~5-7x lower) compared to separately dosed parent drug may potentially reduce C_{max}-driven toxicities. Released drug plasma half-life was extended by ~10-14 fold *vs.* parent. Interestingly, although the *in vivo* total drug levels for the GEM-hexanoate NDC **12c** were slightly higher and may indicate greater stability (*i.e.*, slower release of drug) compared to the glycinate NDC **11c**, the released drug PK curves (including C_{max}) were quite similar for the respective GEM NDCs. This in contrast to the more differentiated total and released drug PK data comparisons between the CBTX-hexanoate and CBTX-glycinate NDCs, which correlated well with *in vitro* release data. This lack of linker-to-linker SAR transferability (and IVIVC) between API drug payloads may be due to a "customization" of NDC *in vivo*

release profiles, driven by both API payload (i.e., local steric and electronic structural environment) and linker functionality. However, it's also known that lower loaded NDCs (~50% of theoretical) accelerate the *in vivo* release of drug from the nanoparticles, reflected by increases in released drug AUC.[41] So it is possible that the lower loaded, faster releasing GEM NDCs overcome any structural differentiation imparted by their linkers, resulting in an *in vivo* released drug normalization effect.

An additional difference between the CBTX and GEM NDCs is the higher availability of released GEM in systemic circulation after NDC dosing (*i.e.*, % AUC of separately dosed parent GEM), which is much greater than 100% (F = ~500-600%). This would indicate either Cl or distribution of the API is affected by GEM NDC administration. A possible explanation for the former is that encapsulation of the GEM drug payload in the NDC protects it from extensive deamination, resulting in greater AUC (and decreased Cl) of released active drug compared to separately dosed GEM.

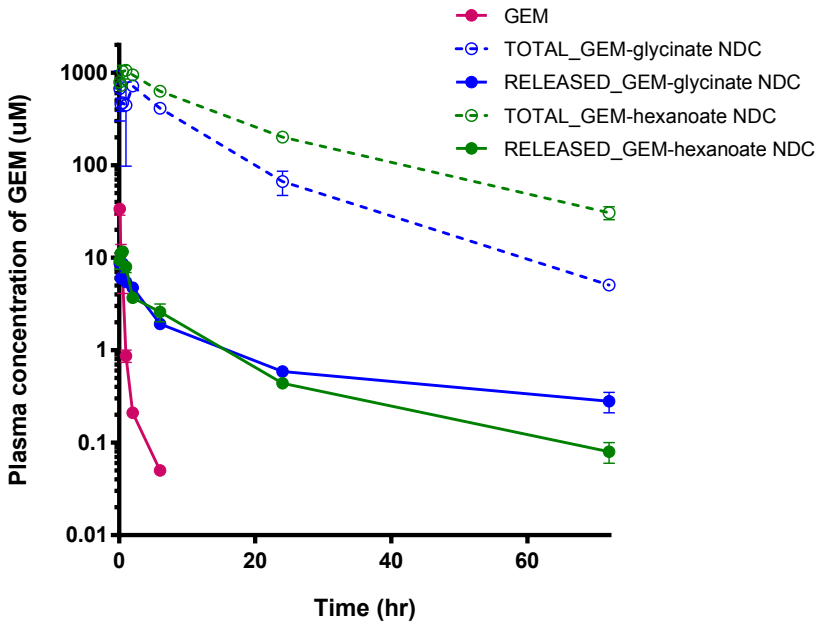

Figure 5. *In vivo* plasma exposure profiles comparing separately dosed GEM to total and released GEM from GEM-glycinate **11c** and GEM-hexanoate **12c** NDCs after a single iv dose of 10 mg/kg each given to non-tumor bearing male C57BL/6 mice.

Table 4. Plasma PK parameters after a single iv dose of 10 mg/kg GEM, GEM-glycinate NDC **11c** or GEM-hexanoate NDC **12c** was given to male C57BL/6 mice.

Test Article		**AUC_∞** [μM*h]	**C_0** or **C_{max}** [μM]	**t_{max}** [hr]	**Cl** [mL/min/kg]	**$t_{1/2}$** [h]	**V_D**[a] [L/kg]	**F**[b] [%]
GEM		12	59	-	55	1.3	1.5	-
GEM-glycinate NDC	Total	7466	820	-	0.087	11	0.02	-
	Released	75	8.8	0.08	-	18	-	625
GEM-hexanoate NDC	Total	16894	830	-	0.037	16	0.05	-
	Released	62	12	0.5	-	13	-	517

[a] V_D is calculated as V_{ss} (estimated volume of distribution at steady state) for nanoparticles dosed iv. [b]F = availability of administered GEM dose in systemic circulation.

2.4. Efficacy Studies of Cabazitaxel NDCs with Glycinate and Hexanoate Linkers

Definitive *in vivo* efficacy studies for the CBTX NDCs were conducted in mouse tumor models to determine the impact of sustained drug release (via NDC) in plasma/tumors on efficacy and survival compared to parent drug in a multi-day study setting. Given the differentiated and favorable PK profiles (plasma and tumor) for the CBTX-glycinate **1c** and CBTX-hexanoate **2c** NDCs, both were selected for the efficacy studies. Dosing was based on the respective maximum tolerated dose (MTD) of each treatment, determined as the dose that caused <20% mean body weight loss in tumor-bearing mice after qwx2 dosing,

which was determined *a priori* to be slightly higher for the more stable CBTX-hexanoate NDC **2c** than the faster releasing CBTX-glycinate NDC **1c** and CBTX parent drug. Male mice carrying the taxane-resistant B16.F10 melanoma syngeneic tumors were given two iv weekly treatments (qwx2) of either the CBTX-glycinate (24 mg/kg) or CBTX-hexanoate (30 mg/kg) NDCs or CBTX (24 mg/kg); the vehicle solution arm was used as a negative control. Tumor growth continued exponentially, from the initial average tumor size of 60 mm^3, for the vehicle control as well as CBTX parent drug after 6 and 12 days, respectively (Fig. 6A). In contrast, tumor growth was inhibited up to Day-30 (18 days post last dose) for CBTX-glycinate NDC **1c** and up to Day-44 (32 days post last dose) for CBTX-hexanoate NDC **2c**. The demonstrated efficacy in the mouse tumor model for the NDCs is supported by the high and sustained levels of both released (efficacious) and total drug (driving released drug levels) in tumor, as shown in the B16.F10 PK study. The corresponding survival curves from the efficacy study showed significant improvement over the 50-day experiment for the NDCs compared to vehicle and parent drug (Fig. 6B), with nearly 100% survival for the CBTX-hexanoate NDC **2c**. The overall optimal efficacy profile of the CBTX-hexanoate NDC **2c** can be explained by its plasma and tumor PK. This PK profile, providing substantially (>10x) reduced plasma C_{max} and increased tumor half-life for released drug *vs.* parent, allowed for a more tolerated and higher efficacious dose (>4x projected tumor AUC *vs.* parent drug) with greater sustained drug release to be delivered in the *in vivo* tumor model.

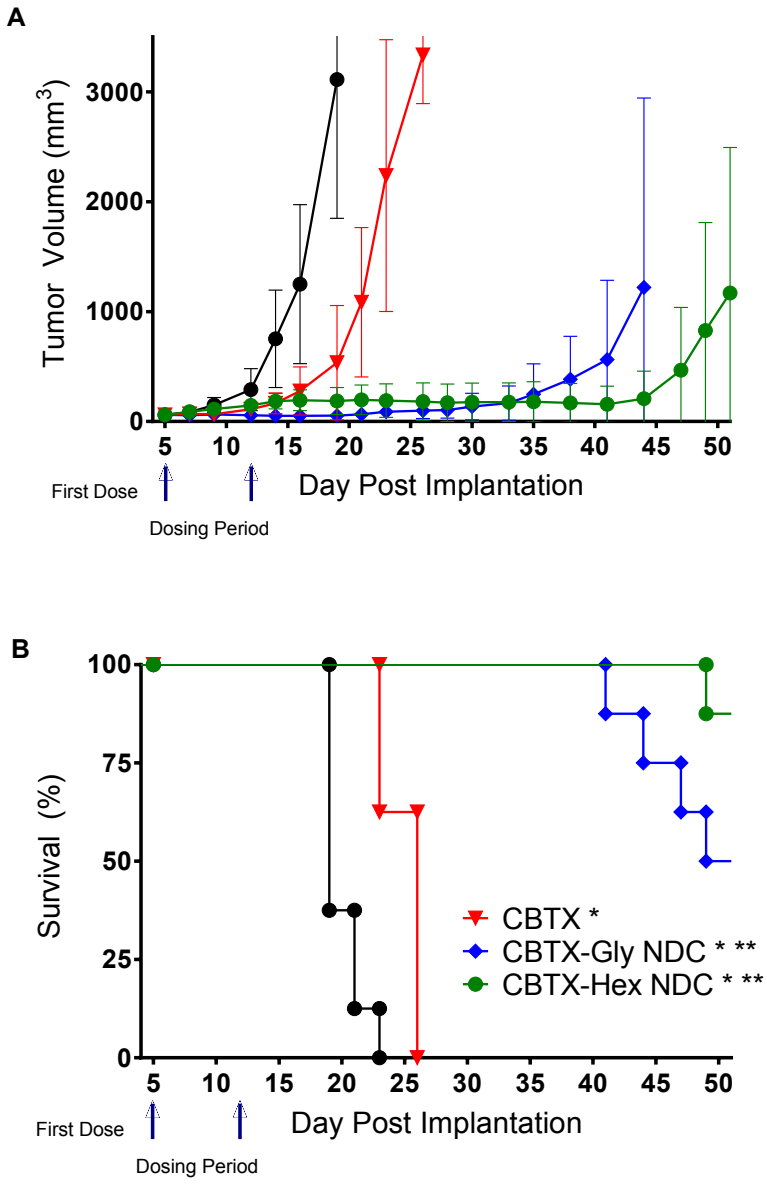

Figure 6. *In vivo* efficacy and survival graphs. (A) Efficacy graph of CBTX (24 mg/kg) as well as CBTX-glycinate **1c** (24 mg/kg) and CBTX-hexanoate **2c** (30 mg/kg) NDCs after two weekly doses (iv, qwx2) in male mice carrying B16.F10 melanoma syngeneic tumors. (B) Corresponding survival curves from B16.F10 efficacy study. Log-rank test used for statistical analysis and showed there was a statistically significant time-to-event difference between vehicle and the CBTX, CBTX-glycinate, CBTX-hexanoate groups with a *p-value < 0.0001, and a statistically significant time-to-event difference between CBTX and the CBTX-glycinate, CBTX-hexanoate groups with a **p-value < 0.0001. Black circles represent the vehicle solution as control.

A second efficacy study was conducted in male mice carrying UISO-BCA-1 breast xenograft tumors, a tumor line that has shown resistance to docetaxel treatment.[57] The mice were given two weekly doses (iv, qwx2) of CBTX (24 mg/kg) as well as CBTX-glycinate **1c** (18 mg/kg) and CBTX-hexanoate **2c** (30 mg/kg) NDCs. As in the first study, the dose levels were based on the differing MTDs measured for the compounds; albeit a slightly lower MTD was obtained for the CBTX-glycinate NDC **1c** in this tumor model. Signs of tumor regrowth occurred for some mice (2 of 8) around Day-90 for the group treated with parent drug CBTX, in contrast to tumor regression and tumor growth delay out to Day-130 for 100% of mice treated with the CBTX-glycinate NDC **1c** (Fig. 7A). Remarkably, tumors treated with the CBTX-hexanoate NDC **2c** showed growth from average tumor size of 170 mm^3 to about 330 mm^3 during the initial stages of treatment, before tumor sizes decreased considerably by Day 37 (with no additional treatment). This resulted in 100% of the mice tumor-free (*i.e.*, tumor free survival, TFS) for the remainder of the 149-day experiment for the CBTX-hexanoate NDC **2c**. Both CBTX NDCs demonstrated greater tumor growth delay *vs.* parent drug in this tumor model, and the more stable hexanoate NDC **2c** led to 100% survival at Day 149 as shown in the corresponding efficacy survival curves (Fig. 7B).

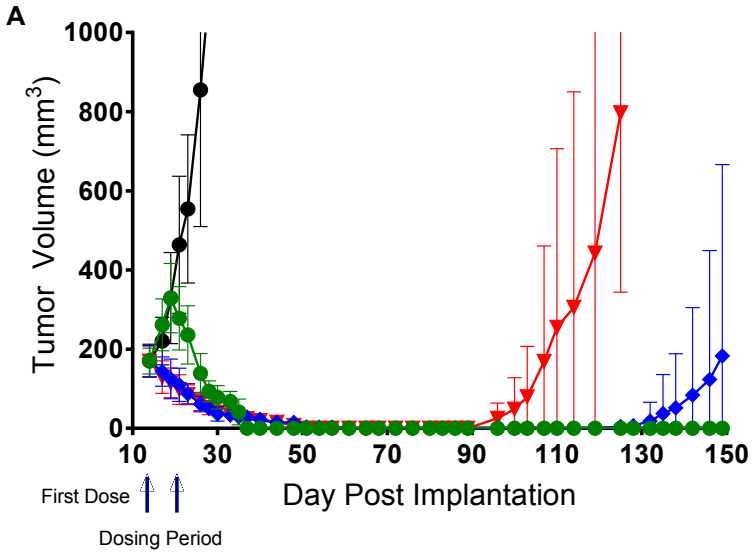

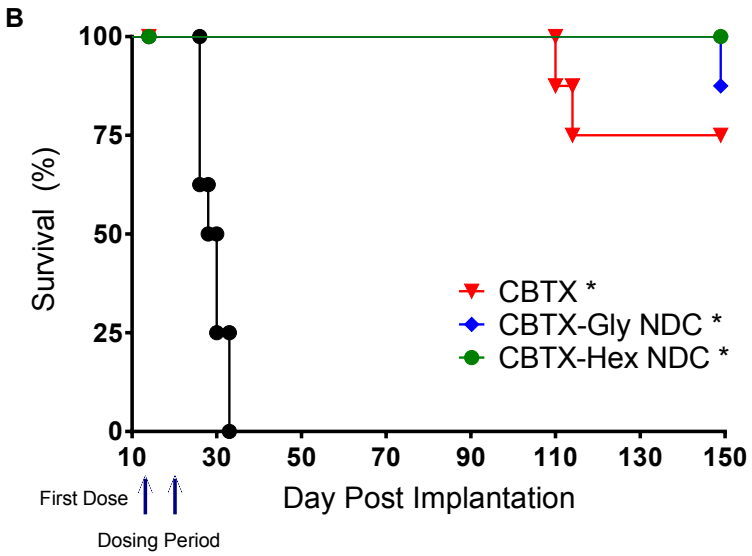

Figure 7. *In vivo* efficacy and survival graphs. (A) Efficacy graph of CBTX (24 mg/kg) as well as CBTX-glycinate **1c** (18 mg/kg) and CBTX-hexanoate **2c** (30 mg/kg) NDCs after two weekly doses (iv, qwx2) in male mice carrying UISO-BCA-1 breast xenograft tumors. (B) Corresponding survival curves from UISO-BCA-1 efficacy study. Log-rank test used for statistical analysis and showed there was a statistically significant time-to-event difference between vehicle and the CBTX, CBTX-glycinate, CBTX-hexanoate groups with a *p-value < 0.0001. Black circles represent the vehicle solution as control.

3. Conclusions

We have demonstrated that diverse API payloads (docetaxel, cabazitaxel, and gemcitabine) with a range of physicochemical properties (*e.g.*, MW, lipophilicity, and aq solubility) can be conjugated via a variety of linkers to a β-cyclodextrin-PEG (CDP) copolymer backbone. Using this technology, we were able to fine tune *in vitro* and *in vivo* drug release kinetics that led to the generation of two optimized NDCs, CBTX-hexanoate **2c** and CBTX-glycinate **1c**. The *in vitro* release data for the CBTX NDCs provided predictable IVIVC correlation on a "rank-order" level, driven by the differentiated release rates of the linkers. Studies in native and heat-inactivated plasma had no influence on the release kinetics, indicating

that drug release was likely pH- but not enzyme-triggered. By taking advantage of the strengths of the NDC linker technology (i.e., tunable release rates based on linker design) we were able to provide differentiated and improved PK profiles for both CBTX NDCs, particularly in plasma, as exemplified in the B16.F10 PK study. The result was lower C_{max} (~4-50x) for released drug in plasma and vastly reduced (~200-900x) volume of distribution and clearance of total drug for both the CBTX- glycinate **1c** and CBTX- hexanoate **2c** NDCs (moreso) compared to separately dosed parent drug. In tumor, both NDCs provided increased (*vs.* parent) tumor exposure of total drug (~8-30x); however, only CBTX-hexanoate NDC **2c** provided a substantial increase in released drug AUC (3-4x) and half-life (>10x) *vs.* CBTX. CBTX-hexanoate NDC **2c** also demonstrated an impressive released drug tumor-to-plasma AUC ratio of 40:1. Increases in released drug plasma half-life over parent drug (e.g., >10x for the GEM NDCs) support the use of the NDC platform as a half-life extension technology. The CBTX NDCs demonstrated improved *in vivo* efficacy compared to CBTX parent drug. CBTX-hexanoate NDC **2c** (CRLX522) provided an optimal overall *in vivo* PK and efficacy/safety profile as demonstrated by greater tumor growth delay *vs.* parent in both efficacy models, 100% TFS in the UISO-BCA-1 model, significantly enhanced survival *vs.* parent in the B16.F10 model (≥ 88% survival in both models), and higher MTD. The results support further evaluation of CRLX522 as a potential anticancer therapeutic agent. In conclusion, the studies presented here demonstrate the utility and diversity of the NDC linker technology platform and pave the way for future evolution of the NDC platform, to include the conjugation of multiple payloads to a single NDC and the development of antibody-conjugated NDCs.[61-63]

4. Experimental Section

4.1. Materials

Acetonitrile (ACN) HPLC grade or equivalent, N-*tert*-butoxycarbonyl-alanine (Boc-alanine), N-*tert*-butoxycarbonyl-β-alanine-OH (Boc-β-alanine-OH), N-*tert*-butoxycarbonyl-6-aminohexanoic acid (Boc-

aminohexanoic acid), N-*tert*-butoxycarbonyl-glycine (Boc-glycine), tert-butyl bromoacetate, cabazitaxel (CBTX, Tecoland Co.), N-carbobenzoxy-alanine (Cbz-alanine), N-carbobenzoxy-6-aminohexanoic acid (Cbz-aminohexanoic acid), N-carbobenzoxy-glycine (Cbz-glycine), charcoal Darco® 175, β-cyclodextrin-PEG (CDP, Cerulean Pharma Inc.) copolymer, dichloroacetic acid (DCA), dichloromethane (DCM), N,N-diisopropylethylamine (DIEA), N-(3-dimethylaminopropyl)-N′-ethylcarbodiimide hydrochloride (EDC·HCl), 4-(dimethylamino)pyridine (DMAP), N,N-dimethylformamide (DMF), docetaxel (DTX, LGM Pharma), formic acid (99+%), gemcitabine (GEM, Bosche Scientific), heptanes, N-hydroxysuccinimide (NHS), magnesium sulfate ($MgSO_4$), methanesulfonic acid (MSA), methanol (MeOH) HPLC grade or equivalent, 4-methoxytriphenylmethyl chloride (MMT-Cl), palladium on carbon (10% Pd/C), sodium sulfate (Na_2SO_4), trifluoroacetic acid (TFA), water HPLC grade or equivalent. All chemicals purchased from Sigma-Aldrich unless noted otherwise.

4.2. Analytical Methods

Analytical HPLC analyses for (i) NDC drug concentration, loading and purity, and (ii) small molecule purity levels were conducted using: (i) an Agilent 1200, a photodiode array (PDA) detector, a Zorbax 300SB-C18 or YMCpac CN300 column, multiple gradients using water/(acetonitrile/methanol) mobile phases with 0.1% of formic acid or 0.5% TFA; (ii) a Waters 2695, ultraviolet (UV) detection at 230 nm, a column Agilent Zorbax Eclipse XTD-C8, a linear gradient from 5% to 99% B (mobile phase A = water + 0.1% TFA and B = ACN + 0.1% TFA) or an Agilent 1200, a PDA detector, a C18 column, a linear gradient from 5% to 95% B (mobile phase A = water + 0.1% formic acid and B = ACN + 0.1% formic acid). The concentration of solid material was determined using an oven gravimetric method. Drug loading was calculated based on concentration of drug *vs.* total solids. Particle size for NDCs was measured in water using a Malvern Zetasizer Nano ZS dynamic light scattering instrument and automatic settings. The original sample was diluted to reach a concentration of solids in the suspension of 5 mg/mL level (mass of a solid estimated based on gravimetric method) using appropriate viscosity values. Proton magnetic resonance spectra were recorded on either a Varian Inova 400 MHz or a Brüker Avance 300 MHz spectrometer. MS

spectra were recorded on either a PE SCIEX, API 150EX (HPLC – SHIMADZU SCL-10A with LC-10AD pumps) or an Agilent 6410 mass spectrometer. Automated flash chromatography was performed using either an Agilent 971-FP purification system with RediSep Rf Gold Silica Flash Chromatography columns (20-40 μm) or a Combiflash system - Companion XL with Foxy200 fraction collector. Tangential Flow Filtration (TFF) purification of NDCs was preformed using a Pall Minimate System with a Millipore Pellicon XL 30kDa cartridge. DLS characterization, concentration, loading, and purity data for the final generated NDCs are provided in Table 1. Purities for final NDC SAR test compounds are ≥ 95.0% and the analytical methods used to determine purity are as follows: an Agilent 1200 with a PDA detector and a Zorbax 300SB-C18 (CBTX, DTX NDCs) or YMCpac CN300 column (GEM NDCs), using multiple gradients and water/(acetonitrile/methanol) mobile phases with 0.1% of formic acid (CBTX, DTX) or 0.5% TFA (GEM).

4.3.1. Syntheses of Cabazitaxel NDCs

(2aR,4S,4aS,6R,9S,11S,12S,12aR,12bS)-12b-Acetoxy-9-(((2R,3S)-2-((((benzyloxy)carbonyl)glycyl)oxy)-3-((tert-butoxycarbonyl)amino)-3-phenylpropanoyl)oxy)-11-hydroxy-4,6-dimethoxy-4a,8,13,13-tetramethyl-5-oxo-2a,3,4,4a,5,6,9,10,11,12,12a,12b-dodecahydro-1H-7,11-methanocyclodeca[3,4]benzo[1,2-b]oxet-12-yl benzoate (1a). Cbz-glycine (0.58 g, 2.8 mmol), CBTX (2.0 g, 2.4 mmol) and DMAP (0.35 g, 2.9 mmol) were dissolved in DCM (20 mL), then EDC·HCl (0.55 g, 2.9 mmol) was added. The reaction stirred at RT overnight. The reaction mixture was diluted with DCM (50 mL) and washed with water (2 x 50 mL) followed by brine (50 mL). The solvent was removed under vacuum and the residue was purified by flash SiO_2 chromatography eluting with a gradient of 0 –5 % DCM:MeOH to furnish a white solid (2.2 g, 90 % yield). ^{1}H NMR (δ ppm, DMSO-*d*6): 0.95 (s, 3H), 0.97 (s, 3H), 1.37 (s, 9H), 1.49 (m, 4H), 1.77 (m, 3H), 2.23 (s, 3H), 2.65 (m, 1H), 3.20 (s, 3H), 3.56 (d, J = 6.9 Hz, 1H), 3.74 (m, 1H), 3.90 (t, J = 5.4 Hz, 1H), 4.00 (s, 2H), 4.48 (s, 1H), 4.68 (s, 1H), 4.94 (d, J = 9.6 Hz, 1H), 5.05-5.11 (m, 4H), 5.36 (d, J = 6.9 Hz, 1H), 5.88 (t, J = 8.8 Hz, 1H), 7.19 (t, J = 7.1 Hz, 1H), 7.29-

7.43 (br m, 9H), 7.65 (t, *J* = 7.6 Hz, 2H), 7.72 (d, *J* = 7.1 Hz, 1H), 7.76 (t, *J* = 6 Hz, 1H), 7.90 (d, *J* = 8.9 Hz, 1H), 7.97 (d, *J* = 7.6 Hz, 2H).

(2aR,4S,4aS,6R,9S,11S,12S,12aR,12bS)-12b-Acetoxy-9-(((2R,3S)-3-((tert-butoxycarbonyl)amino)-2-(glycyloxy)-3-phenylpropanoyl)oxy)-11-hydroxy-4,6-dimethoxy-4a,8,13,13-tetramethyl-5-oxo-2a,3,4,4a,5,6,9,10,11,12,12a,12b-dodecahydro-1H-7,11-methanocyclodeca[3,4]benzo[1,2-b]oxet-12-yl benzoate (1b). Compound **1a** (2.1 g, 2.0 mmol) was dissolved in THF (44 mL) and MeOH (1.3 mL) followed by the addition of methane sulfonic acid (0.18 g, 1.8 mmol) and 10 % Pd/C (0.68 g). The solution was placed in a hydrogen reactor (30 PSI) for 1 h. The solids were removed by filtration through a Celite pad. Precipitation from heptanes at ambient temperature gave the desired CBTX-glycinate as an off-white solid (1.7 g, 85 % yield). ^{1}H NMR (δ ppm, DMSO-*d*6): 0.97 (s, 3H), 0.98 (s, 3H), 1.36 (s, 9H), 1.50 (m, 4H), 1.82 (m, 3H), 2.27 (s, 3H), 2.29 (s, 2H), 2.65 (m, 1H), 3.20 (s, 3H), 3.59 (d, *J* = 6.7 Hz, 1H), 3.73 (m, 1H), 3.86 (m, 1H), 4.02 (s, 2H), 4.53 (s, 1H), 4.69 (s, 1H), 4.95 (d, *J* = 9.8 Hz, 1H), 5.13-5.18 (m, 2H), 5.38 (d, *J* = 7.1 Hz, 1H), 5.87 (t, *J* = 7.6 Hz, 1H), 7.21 (t, *J* = 6.5 Hz, 1H), 7.36-7.45 (br m, 4H), 7.64 (t, *J* = 7.6 Hz, 2H), 7.71 (d, *J* = 7.4 Hz, 1H), 7.88 (d, *J* = 8.5 Hz, 1H), 7.99 (d, *J* = 7.4 Hz, 2H). MS m/z calculated for $C_{47}H_{60}N_2O_{15}$, 892.40, found $[M+H]^+$, 893.4.

CBTX-glycinate NDC (1c). CDP copolymer (2.0 g, 0.41 mmol) in dry DMF (20 mL), **1b** (0.90 g, 0.91 mmol), EDC·HCl (0.17 g, 0.91 mmol), NHS (0.10 g, 0.91 mmol), and DIEA (0.12 g, 0.91 mmol) were mixed for 2 hours and the polymer conjugate was precipitated into IPA (300 mL). The IPA was decanted and the beaker was charged with acetone (150 mL). After stirring for 15 minutes the acetone was decanted and residual polymer was dissolved in pH 3 water (200 mL). The crude CBTX-glycinate-NDC was purified by TFF in pH 3 water (30k MWCO regenerated cellulose membrane). The retentate was concentrated (80 mL), filtered through Millipore Steriflip 0.22-µm filter, and the resulting NDC aqueous solution was stored at -20 °C. See Table 1 for DLS characterization, concentration, loading, and purity data.

(2aR,4S,4aS,6R,9S,11S,12S,12aR,12bS)-12b-Acetoxy-9-(((2R,3S)-2-((6-(((benzyloxy)carbonyl)amino)hexanoyl)oxy)-3-((tert-butoxycarbonyl)amino)-3-phenylpropanoyl)oxy)-11-hydroxy-4,6-dimethoxy-4a,8,13,13-tetramethyl-5-oxo-2a,3,4,4a,5,6,9,10,11,12,12a,12b-dodecahydro-1H-7,11-methanocyclodeca[3,4]benzo[1,2-b]oxet-12-yl benzoate (2a). The synthesis of **2a** was carried out as described above for **1a** using Cbz-6-aminohexanoic acid (0.73 g, 2.8 mmol), CBTX (2.0 g, 2.4 mmol), DMAP (0.35 g, 2.9 mmol), DCM (50 mL), and EDC·HCl (0.55 g, 2.9 mmol). The product was recovered as a white solid (2.4 g, 92 % yield). ^{1}H NMR (δ ppm, DMSO-*d*6): 0.95 (s, 3H), 0.96 (s, 3H), 1.23 (m, 3H), 1.36 (m, 11H), 1.49-1.56 (br m, 8H), 1.78 (s, 4H), 2.07 (s, 2H), 2.23 (s, 3H), 2.37 (t, *J* = 7.1 Hz, 2H), 2.65 (m, 1H), 2.97 (q, *J* = 6.6 Hz, 2H), 3.19 (s, 3H), 3.57 (d, *J* = 7Hz, 1H), 3.74 (m, 1H), 4.00 (m, 3H), 4.48 (s, 1H), 4.68 (s, 1H), 4.94 (d, *J* = 9.6, 1H), 5.00 (s, 2H), 5.06 (t, *J* = 6.8 Hz, 2H), 5.35 (d, *J* = 7.2 Hz, 1H), 5.79 (t, *J* = 8.6 Hz, 1H), 7.16 (t, *J* = 7.2 Hz, 1H), 7.23 (t, *J* = 5.9 Hz, 1H), 7.29-7.43 (br m, 10H), 7.64 (t, *J* = 7.2 Hz, 2H), 7.72 (t, *J* = 7.5 Hz, 1H), 7.85 (d, *J* = 8.1 Hz, 1H, 7.96 (d, *J* = 7.1 Hz, 2H).

(2aR,4S,4aS,6R,9S,11S,12S,12aR,12bS)-12b-Acetoxy-9-(((2R,3S)-2-((6-aminohexanoyl)oxy)-3-((tert-butoxycarbonyl)amino)-3-phenylpropanoyl)oxy)-11-hydroxy-4,6-dimethoxy-4a,8,13,13-tetramethyl-5-oxo-2a,3,4,4a,5,6,9,10,11,12,12a,12b-dodecahydro-1H-7,11-methanocyclodeca[3,4]benzo[1,2-b]oxet-12-yl benzoate (2b). Compound **2b** was prepared as described for compound **1b** using compound **2a** (2.4 g, 2.2 mmol). The product was recovered as an-off white solid (1.5 g, 65 % yield). ^{1}H NMR (δ ppm, DMSO-*d*6): 0.95 (s, 3H), 0.96 (s, 3H), 1.16-1.37 (br m, 13H), 1.45-1.57 (br m, 9H), 1.78 (s, 4H), 2.23 (s, 3H), 2.31 (s, 3H), 2.39 (t, *J* = 7.1 Hz, 2H), 2.64 (m, 1H), 2.74 (t, *J* = 7.6 Hz, 2H), 3.20 (s, 3H), 3.56 (d, *J* = 7.3 Hz, 1H), 3.73 (m, 1H), 4.00 (s, 2H), 4.48 (s, 1H), 4.67 (s, 1H), 4.94 (d, *J* = 10.1 Hz, 1H), 5.06 (m, 2H), 5.35 (d, *J* = 7.1 Hz, 1H), 5.79 (t, *J* = 8.7 Hz, 1H), 7.16 (t, *J* = 7.2 Hz, 1H), 7.34-7.44 (br m, 5H), 7.65 (t, *J* = 7.5 Hz, 2H), 7.73 (t, *J* = 7.0 Hz, 1H), 7.87 (d, *J* = 8.5 Hz, 1H), 7.97 (d, *J* = 7.0 Hz, 2H). MS m/z calculated for $C_{51}H_{68}N_2O_{15}$, 948.46, found $[M+H]^+$, 949.5.

CBTX-hexanoate NDC (2c). Compound **2c** was prepared as described for compound **1c** using CDP copolymer (2.0 g, 0.41 mmol) in dry DMF (20 mL), **2b** (0.95 g, 0.91 mmol), EDC·HCl (0.17 g, 0.91 mmol), NHS (0.10 g, 0.91 mmol), and DIEA (0.12 g, 0.91 mmol). See Table 1 for DLS characterization, concentration, loading, and purity data.

(2aR,4S,4aS,6R,9S,11S,12S,12aR,12bS)-12b-Acetoxy-9-(((2R,3S)-2-((((benzyloxy)carbonyl)-L-alanyl)oxy)-3-((tert-butoxycarbonyl)amino)-3-phenylpropanoyl)oxy)-11-hydroxy-4,6-dimethoxy-4a,8,13,13-tetramethyl-5-oxo-2a,3,4,4a,5,6,9,10,11,12,12a,12b-dodecahydro-1H-7,11-methanocyclodeca[3,4]benzo[1,2-b]oxet-12-yl benzoate (3a). Compound **3a** was prepared as described for compound **1a** using Cbz-alanine (0.61 g, 2.8 mmol), CBTX (2.0 g, 2.4 mmol), DMAP (0.35 g, 2.9 mmol), DCM (50 mL), and EDC·HCl (0.55 g, 2.9 mmol). The product was recovered as a white solid (2.5 g, 99 % yield). ^{1}H NMR (δ ppm, DMSO-*d*6): 0.97 (s, 3H), 0.99 (s, 3H), 1.31 (m, 3H), 1.36 (s, 9H), 1.51 (m, 4H), 1.77 (s, 2H), 2.29 (s, 3H), 2.66 (m, 1H), 3.20 (s, 3H), 3.60 (d, *J* = 6.8 Hz, 1H), 3.76 (m, 1H), 4.02 (s, 2H), 4.26 (t, *J* = 7.6 Hz, 1H), 4.52 (s, 1H), 4.68 (s, 1H), 4.96 (d, *J* = 9.6 Hz, 1H), 5.03 (d, *J* = 6.5 Hz, 2H), 5.11-5.16 (br m, 2H), 5.38 (d, *J* = 7.2 Hz, 2H), 5.88 (t, *J* = 8.8 Hz, 1H), 7.19 (m, 1H), 7.31-7.42 (br m, 9H), 7.64 (t, *J* = 7.2 Hz, 2H), 7.71 (t, *J* = 7.0 Hz, 1H), 7.81 (d, *J* = 7.5 Hz, 1H), 7.92 (d, *J* = 9.5 Hz, 1H), 7.98 (d, *J* = 7.3 Hz, 2H).

(2aR,4S,4aS,6R,9S,11S,12S,12aR,12bS)-9-(((2R,3S)-2-((L-Alanyl)oxy)-3-((tert-butoxycarbonyl)amino)-3-phenylpropanoyl)oxy)-12b-acetoxy-11-hydroxy-4,6-dimethoxy-4a,8,13,13-tetramethyl-5-oxo-2a,3,4,4a,5,6,9,10,11,12,12a,12b-dodecahydro-1H-7,11-methanocyclodeca[3,4]benzo[1,2-b]oxet-12-yl benzoate (3b). Compound **3b** was prepared as described for compound **1b** using compound **3a** (2.4 g, 2.2 mmol). The product was recovered as an off-white solid (1.7 g, 74 % yield). ^{1}H NMR (δ ppm, DMSO-*d*6): 0.97 (s, 3H), 0.99 (s, 3H), 1.23 (m, 2H), 1.36 (s, 9H), 1.41 (m, 3H), 1.50 (m, 4H), 1.82 (m, 3H), 2.27 (s, 3H), 2.33 (s, 3H), 2.65 (m, 1H), 3.20 (s, 3H), 3.59 (d, *J* = 6.7 Hz, 1H), 3.74 (m, 1H), 4.02 (s, 2H), 4.26 (q, *J* = 7.5 Hz, 1H), 4.53 (s, 1H), 4.69 (s, 1H), 4.95 (d, *J* = 9.7 Hz, 1H), 5.19 (m, 2H), 5.38 (d, *J* = 7.1 Hz, 1H), 5.88 (t, *J* = 9.3 Hz, 1H), 7.21 (t, *J* = 7.1 Hz, 1H), 7.37-

7.46 (m, 4H), 7.64 (t, *J* = 7.0 Hz, 2H), 7.72 (t, *J* = 7.4 Hz, 1H), 7.98 (m, 3H). MS m/z calculated for $C_{48}H_{62}N_2O_{15}$, 906.42, found $[M+H]^+$, 907.4.

CBTX-alaninate NDC (3c.) Compound **3c** was prepared as described for compound **1c** using CDP copolymer (2.0 g, 0.41 mmol) in dry DMF (20 mL), **3b** (0.91 g, 0.91 mmol), EDC·HCl (0.17 g, 0.91 mmol), NHS (0.11 g, 0.91 mmol), and DIEA (0.12 g, 0.91 mmol). See Table 1 for DLS characterization, concentration, loading, and purity data.

2-((2-(((4-Methoxyphenyl)diphenylmethyl)amino)ethyl)disulfanyl)ethan-1-ol (4). Cystamine dihydrochloride (5.0 g, 22 mmol), TEA (4.5 mL, 32 mmol), and MMT-Cl (12 g, 40 mmol) were reacted in DCM. Crude N,N'-bis(4-methoxytrityl) cystamine (MMT-NHEt-SS-EtNH-MMT) was isolated and purified by column chromatography using 0 – 100 % Hexanes:EtOAc as the eluent to yield white solid (12 g, 80% yield). ^{1}H NMR (δ ppm, DMSO-*d*6): 2.23 (q, *J* = 7.1 Hz, 4H), 2.71 (t, *J* = 7.6 Hz, 4H), 3.69 (s, 6H), 6.80-6.87 (m, 4H), 7.00-7.29 (br m, 18H), 7.39 (d, *J* = 7.6 Hz, 6H). MMT-NHEt-SS-EtNH-MMT (5.6 g, 8.0 mmol), 2-mercaptoethanol (0.63 g, 8.0 mmol) and 2-hydroxyethyldisulfide (6.2 g, 40 mmol) were reacted in MeOH:DCM 1:1. Crude N-(4-methoxytrityl)-2-[(2-aminoethyl)dithio]ethanol] (MMT-NHEt-SS-ethanol) was separated, dissolved in DCM, and treated with iodine (I_2). The resulting oil was isolated and column-purified using 0 – 100 % DCM:EtOAc to yield MMT-NHEt-SS-ethanol as clear oil (890 mg, 45 % yield). ^{1}H NMR (δ ppm, DMSO-*d*6): 2.28 (q, *J* = 7.2 Hz, 2H), 2.67 (t, *J* = 6.7 Hz, 2H), 2.85 (t, *J* = 6.6 Hz, 2H), 3.57 (q, *J* = 5.9 Hz, 2H), 3.72 (s, 3H), 4.83 (t, *J* = 5.7 Hz, 1H), 6.86 (d, *J* = 9.0 Hz, 2H), 7.18 (t, *J* = 7.2 Hz, 2H), 7.27-7.31 (m, 6H), 7.41 (d, *J* = 7.4 Hz, 4H).

(2aR,4S,4aS,6R,9S,11S,12S,12aR,12bS)-12b-Acetoxy-9-(((R)-12-((S)-((tert-butoxycarbonyl)amino)(phenyl)methyl)-1-(4-methoxyphenyl)-10-oxo-1,1-diphenyl-9,11-dioxa-5,6-dithia-2-azatridecan-13-oyl)oxy)-11-hydroxy-4,6-dimethoxy-4a,8,13,13-tetramethyl-5-oxo-2a,3,4,4a,5,6,9,10,11,12,12a,12b-dodecahydro-1H-7,11-methanocyclodeca[3,4]benzo[1,2-b]oxet-12-yl benzoate (4a). Compound **4** (1.1 g, 2.7 mmol), disuccinimidyl carbonate (0.82 g, 3.2 mmol) and TEA (0.27

g, 27 mmol) were dissolved in ACN and mixed with a solution of CBTX (2.0 g, 2.4 mmol) and DMAP (0.32 g, 2.7 mmol) in DCM. After complete reaction as monitored by HPLC for residual CBTX, the mixture was concentrated and purified by column chromatography using 0 – 100 % DCM:EtOAc to produce the desired product as a white solid (1.1 g, 35 % yield). ^{1}H NMR (δ ppm, DMSO-*d*6): 0.96 (s, 3H), 0.97 (s, 3H), 1.35 (s, 9H), 1.49 (m, 4H), 1.80 (m, 3H), 2.24 (s, 3H), 2.28 (q, *J* = 7.2 Hz, 2H), 2.64 (m, 1H), 2.81-2.89 (br m, 5H), 3.25 (s, 3H), 3.57 (d, *J* = 7.3 Hz, 1H), 4.00 (s, 2H), 4.31 (t, *J* = 6.1 Hz, 2H), 4.94 (s, 1H), 4.68 (s, 1H), 4.94 (d, *J* = 9.8 Hz, 1H), 5.06 (m, 2H), 5.36 (d, *J* = 7.2 Hz, 1H), 5.82 (t, *J* = 8.8 Hz, 1H), 6.85 (d, *J* = 9.4 Hz, 2H), 7.17 (t, *J* = 7.1 Hz, 3H), 7.26-7.29 (m, 7H), 7.34-7.43 (m, 8H), 7.64 (t, *J* = 7.7 Hz, 2H), 7.71 (t, *J* = 7.2 Hz, 1H), 7.93 (d, *J* = 8.8 Hz, 1H), 7.97 (d, *J* = 7.8 Hz, 2H).

(2aR,4S,4aS,6R,9S,11S,12S,12aR,12bS)-12b-Acetoxy-9-(((2R,3S)-2-(((2-((2-aminoethyl)disulfanyl)ethoxy)carbonyl)oxy)-3-((tert-butoxycarbonyl)amino)-3-phenylpropanoyl)oxy)-11-hydroxy-4,6-dimethoxy-4a,8,13,13-tetramethyl-5-oxo-2a,3,4,4a,5,6,9,10,11,12,12a,12b-dodecahydro-1H-7,11-methanocyclodeca[3,4]benzo[1,2-b]oxet-12-yl benzoate (4b). Compound **4a** (1.0 g, 0.78 mmol) was dissolved in a solution of DCM containing anisole (0.84 g, 7.8 mmol) and dichloroacetic acid (640 uL, 7.8 mmol). After stirring at RT for 1 h the DCM reaction was concentrated to 5 mL and precipitated in hexanes (150 mL). The solvents were decanted and the resulting oil was redissolved in THF (10 mL) and precipitated into hexanes (150 mL) to furnish an off-white solid (540 mg, 61 % yield). ^{1}H NMR (δ ppm, DMSO-*d*6): 0.98 (s, 3H), 0.99 (s, 3H), 1.37 (s, 9H), 1.51 (m, 5H), 1.81 (m, 4H), 2.25 (s, 3H), 2.66 (m, 1H), 2.94 (t, *J* = 6.7 Hz, 2H), 3.05 (t, *J* = 6.2 Hz, 2H), 3.11 (t, *J* = 7.2 Hz, 2H), 3.2 (s, 3H), 3.58 (d, *J* = 7.3 Hz, 1H), 3.74 (m 1H), 4.02 (s, 2H), 4.93 (t, *J* = 6.4 Hz, 2H), 4.51 (s, 1H), 4.69 (s, 1H), 4.95 (d, *J* = 8.9 Hz, 1H), 5.06 (m, 2H), 5.37 (d, *J* = 6.6 Hz, 1H), 5.83 (t, *J* = 8.8 Hz, 1H), 6.19 (s, 1H), 7.19 (t, *J* = 6.8 Hz, 1H), 7.34 (m, 3H), 7.44 (t, *J* = 7.1 Hz, 2H), 7.66 (t, *J* = 7.8 Hz, 2H), 7.74 (t, *J* = 6.8 Hz, 1H), 7.97 (m, 3H), 8.02 (br s, 2H). MS m/z calculated for $C_{50}H_{66}N_2O_{16}S_2$, 1014.39, found $[M+H]^+$,1015.3.

CBTX-disulfide NDC (4c). Compound **4c** was prepared as described for compound **1c** using CDP copolymer (1.0 g, 0.41 mmol) in dry DMF (10 mL), **4b** (0.54 g, 0.47 mmol), EDC·HCl (0.090 g, 0.47 mmol), NHS (0.054 g, 0.47 mmol), and DIEA (0.061 g, 0.47 mmol). See Table 1 for DLS characterization, concentration, loading, and purity data.

4.3.2. Syntheses of Docetaxel NDCs

(2aR,4S,4aS,6R,9S,11S,12S,12aR,12bS)-12b-Acetoxy-9-(((2R,3S)-2-((((benzyloxy)carbonyl)glycyl)oxy)-3-((tert-butoxycarbonyl)amino)-3-phenylpropanoyl)oxy)-4,6,11-trihydroxy-4a,8,13,13-tetramethyl-5-oxo-2a,3,4,4a,5,6,9,10,11,12,12a,12b-dodecahydro-1H-7,11-methanocyclodeca[3,4]benzo[1,2-b]oxet-12-yl benzoate (5a). DTX (7.5 g, 9.5 mmol) and Cbz-glycine (1.5 g, 7.2 mmol) were mixed in DCM (100 mL), to which EDC·HCl (1.5 g, 7.8 mmol) and DMAP (0.96 g, 7.8 mmol) were added. After 3 hours, a second portion of Cbz-glycine (0.74 g, 3.5 mmol), EDC·HCl (0.74 g, 3.9 mmol), and DMAP (0.47 g, 3.9 mmol) was added. After an additional three hours the reaction was diluted with DCM and washed with 0.1 % HCl and brine. Purification by column chromatography using 0 - 5% DCM:MeOH gave DTX-glycinate as white solid (4.6 g, 48 % yield). ^{1}H NMR (δ ppm, DMSO-*d*6): 0.98 (s, 6H), 1.38 (s, 9H), 1.52 (s, 4H), 1.69 (s, 4H), 2.24 (m, 4H), 3.62 (m, 2H), 4.02 (m, 2H), 4.05 (m, 3H), 4.92, (d, J = 9.9 Hz, 1H), 5.11 (m, 5H), 5.41 (d, J = 7.2 Hz, 1H), 5.80 (t, J = 8.7, 1H), 7.18 (t, J = 6.9 Hz, 1H), 7.31-7.45 (br m, 9H), 7.64-7.74-7.78 (br m, 4H), 7.89 (d, J = 8.7 Hz, 1H), 7.99 (d, J = 7.2 Hz, 2H).

(2aR,4S,4aS,6R,9S,11S,12S,12aR,12bS)-12b-Acetoxy-9-(((2R,3S)-3-((tert-butoxycarbonyl)amino)-2-(glycyloxy)-3-phenylpropanoyl)oxy)-4,6,11-trihydroxy-4a,8,13,13-tetramethyl-5-oxo-2a,3,4,4a,5,6,9,10,11,12,12a,12b-dodecahydro-1H-7,11-methanocyclodeca[3,4]benzo[1,2-b]oxet-12-yl benzoate (5b). Compound **5a** (2.4 g, 2.4 mmol) was dissolved in THF (60 mL). MeOH (2.5 mL), methanesulfonic acid (140 μL, 2.2 mmol), and 5 % Pd/C (0.86 g) were added. The flask was evacuated for 15 seconds and filled with hydrogen gas using a balloon. The

reaction stirred at RT for 3 h and filtered through a Celite pad. The solution was concentrated to 3 mL and heptanes (100 mL) were slowly added to afford a white precipitate. The solid was collected by filtration and dried under vacuum (2.2 g, 95 % yield). ^{1}H NMR (δ ppm, DMSO-*d*6): 0.99 (s, 6H), 1.36 (s, 9H), 1.52 (s, 3H), 1.67 (m, 1H), 1.76 (s, 3H), 1.85 (m, 1H), 2.27 (m, 4H), 3.66 (d, *J* = 6.9 Hz, 1H), 3.81 (m, 2H), 4.03 (m, 4H), 4.92 (d, *J* = 8.7 Hz, 1H), 5.19 (m, 3H), 5.43 (d, *J* = 7.2 Hz, 1H), 5.86 (t, *J* = 8.4 Hz, 1H), 7.22 (t, *J* = 7.2 Hz, 1H), 7.37-7.47 (m, 5H), 7,65 (t, *J* = 7.2 Hz, 2H), 7.73 (d, *J* = 7.2 Hz, 1H), 7.90 (d, *J* = 9.0 Hz, 1H), 8.01 (d, *J* = 7.5 Hz, 2H). MS m/z calculated for $C_{45}H_{56}N_2O_{15}$, 864.37, found $[M+H]^+$ 865.4

DTX-glycinate NDC (5c). Compound **5c** was prepared as described for compound **1c** using CDP copolymer (2.0 g, 0.41 mmol) in dry DMF (20 mL), **5b** (0.88 g, 0.91 mmol), DIEA (0.12 g, 0.91 mmol), EDC·HCl (0.17 g, 0.91 mmol), and NHS (0.11 g, 0.91 mmol). See Table 1 for DLS characterization, concentration, loading, and purity data.

(2aR,4S,4aS,6R,9S,11S,12S,12aR,12bS)-12b-Acetoxy-9-(((2R,3S)-2-((6-(((benzyloxy)carbonyl)amino)hexanoyl)oxy)-3-((tert-butoxycarbonyl)amino)-3-phenylpropanoyl)oxy)-4,6,11-trihydroxy-4a,8,13,13-tetramethyl-5-oxo-2a,3,4,4a,5,6,9,10,11,12,12a,12b-dodecahydro-1H-7,11-methanocyclodeca[3,4]benzo[1,2-b]oxet-12-yl benzoate (6a). Cbz-6-aminohexanoic acid (4.1 g, 16 mmol) and DTX (12 g, 15 mmol) were dissolved in DCM (100 mL) and mixed with EDC·HCl (3.4 g, 18 mmol) and DMAP (2.2 g, 18 mmol). Additional EDC·HCl and DMAP were added until HPLC monitoring indicated 82% conversion with 3 % of remaining DTX. Cbz-hexanoate-DTX was isolated and purified by column chromatography using 90:10 DCM:acetone mixture to afford a white solid (8.6 g, 86 % yield). ^{1}H NMR (δ ppm, DMSO-*d*6): 0.85 (m, 4H), 0.98 (s, 6H), 1.25 (m, 4H), 1.36 (s, 9H), 1.52 (s, 4H), 1.69 (s, 4H), 2.24 (m, 4H), 2.38 (t, *J* = 6.9 Hz, 2H), 2.98 (q, *J* = 6.3 Hz, 2H), 3.62 (d, *J* =6.9 Hz, 1H), 4.02 (m, 2H), 4.05 (m, 3H), 4.91 (d, *J* = 9.6 Hz, 1H), 5.11 (m, 5H), 5.41 (d, *J* = 7.2 Hz, 1H), 5.79 (t, *J* = 8.7 Hz, 1H), 7.17 (t, *J* = 7.2 Hz, 1H), 7.24 (t, *J* = 5.7 Hz, 1H), 7.29-7.35 (m, 9H), 7.63-7.74 (m, 3H), 7.86 (d, *J* = 8.1 Hz, 1H), 7.99 (d, *J* = 6.9 Hz, 2H).

(2aR,4S,4aS,6R,9S,11S,12S,12aR,12bS)-12b-Acetoxy-9-(((2R,3S)-2-((6-aminohexanoyl)oxy)-3-((tert-butoxycarbonyl)amino)-3-phenylpropanoyl)oxy)-4,6,11-trihydroxy-4a,8,13,13-tetramethyl-5-oxo-2a,3,4,4a,5,6,9,10,11,12,12a,12b-dodecahydro-1H-7,11-methanocyclodeca[3,4]benzo[1,2-b]oxet-12-yl benzoate (6b). Compound **6a** (5.3 g, 5.0 mmol) was dissolved in THF (120 mL), then MeOH (5 mL), MSA (320 μL, 4.8 mmol), 5 % Pd/C (1.8 g, 10 mol % of Pd), and a hydrogen balloon were added at 0 °C. The mixture stirred for 3 h and was filtered through a Celite pad, concentrated under vacuum, and diluted with MTBE. The upper clear layer was decanted and the bottom layer filtered through a 0.45 μm filter membrane. The filter cake afforded the product as a white solid (4.2 g, 82 % yield). ^{1}H NMR (δ ppm, DMSO-*d*6): 0.85 (m, 4H), 0.98 (s, 6H), 1.25 (m, 4H), 1.36 (s, 9H), 1.52 (s, 4H), 1.69 (s, 4H), 2.24 (m, 4H), 3.62 (m, 9H), 4.02 (m, 2H), 4.05 (m, 3H), 4.92, (d, J = 9.6 Hz, 1H), 5.11 (m, 3H), 5.41 (d, J = 7.2 Hz, 1H), 5.80 (t, J = 9.0 Hz, 1H), 7.18 (t, J = 6.9 Hz, 1H), 7.31-7.45 (m, 4H), 7.64-7.78 (m, 4H), 7.89 (d, J = 7.2 Hz, 1H), 7.99 (d, J = 7.2 Hz, 2H). MS m/z calculated for $C_{49}H_{64}N_2O_{15}$, 920.43, found $[M+H]^+$ 921.3

DTX-hexanoate NDC (6c). Compound **6c** was prepared as described for compound **1c** using CDP copolymer (2.0 g, 0.41 mmol) in dry DMF (20 mL), **6b** (0.93 g, 0.91 mmol), DIEA (0.12 g, 0.91 mmol), EDC·HCl (0.17 g, 0.91 mmol), and NHS (0.11 g, 0.91 mmol). See Table 1 for DLS characterization, concentration, loading, and purity data.

2-((3-(((Benzyloxy)carbonyl)amino)propanoyl)oxy)acetic acid (7). A 500 mL round-bottom flask equipped with a magnetic stirrer was charged with N-Cbz-β-alanine (30 g, 135 mmol), *tert*-butyl bromoacetate (26 g, 135 mmol), K_2CO_3 (28 g, 203 mmol), and acetone (200 mL). The mixture was refluxed overnight, cooled to ambient temperature, and filtered to remove solid. The filtrate was concentrated under vacuum to afford the desired product as a white solid (45 g, >99 % yield). ^{1}H NMR (δ ppm, $CDCl_3$): 1.47 (s, 9H), 2.64 (t, J = 5.8 Hz, 2H), 3.53 (t, J = 6.0 Hz, 2H), 4.53 (s, 2H), 5.10 (s, 2H), 5.56 (br s, 1H), 7.35 (m, 5H). A 500 mL round-bottom flask equipped with a magnetic stirrer was charged with 2-(tert-butoxy)-2-oxoethyl 3-(((benzyloxy)carbonyl)amino)propanoate (44 g, 130 mmol) and formic acid (100 mL). The mixture was stirred at ambient temperature for 6h and was then concentrated to give a clear oil (33.5 g, 91

% yield). ^{1}H NMR (δ ppm, DMSO-d_6): 2.56 (m, 2H), 3.27 (m, 2H), 4.56 (s, 2H), 5.02 (s, 2H), 7.32 (m, 5H), 13.10 (br s, 1H).

(2aR,4S,4aS,6R,9S,11S,12S,12aR,12bS)-12b-Acetoxy-9-(((R)-12-((S)-((tert-butoxycarbonyl)amino)(phenyl)methyl)-3,7,10-trioxo-1-phenyl-2,8,11-trioxa-4-azatridecan-13-oyl)oxy)-4,6,11-trihydroxy-4a,8,13,13-tetramethyl-5-oxo-2a,3,4,4a,5,6,9,10,11,12,12a,12b-dodecahydro-1H-7,11-methanocyclodeca[3,4]benzo[1,2-b]oxet-12-yl benzoate (7a). Compound **7a** was prepared as described for compound **6a** using DTX (5.0 g, 6.3 mmol), **7** (2.0 g, 7.2 mmol), EDC·HCl (1.5 g, 7.8 mmol) and DMAP (0.75 g, 6.2 mmol) to yield DTX-2'-Cbz-β-alanine-glycolate as white powder (3.5 g, 52% yield). ^{1}H NMR (δ ppm, DMSO-*d*6): 0.98 (s, 6H), 1.37 (s, 9H), 1.51 (s, 4H), 1.68 (s, 4H), 1.85 (m, 1H), 2.23 (m, 4H), 2.59 (t, J = 7.2 Hz, 2H), 3.27 (q, J = 6.0 Hz, 2H), 3.63 (d, J = 7.2 Hz, 1H), 4.03 (m, 3H), 4.44 (s, 1H), 4.78-5.10 (br m, 9H), 5.18 (d, J = 7.8 Hz, 1H), 5.40 (d, J = 7.2 Hz, 1H), 5.78 (t, J = 9.0 Hz, 1H), 7.18 (t, J = 6.9 Hz, 1H), 7.31-7.45 (m, 10H), 7.63-7.73 (m, 3H), 7.89 (d, J = 7.2 Hz, 1H), 7.99 (d, J = 7.2 Hz, 2H).

(2aR,4S,4aS,6R,9S,11S,12S,12aR,12bS)-12b-Acetoxy-9-(((2R,3S)-2-(2-((3-aminopropanoyl)oxy)acetoxy)-3-((tert-butoxycarbonyl)amino)-3-phenylpropanoyl)oxy)-4,6,11-trihydroxy-4a,8,13,13-tetramethyl-5-oxo-2a,3,4,4a,5,6,9,10,11,12,12a,12b-dodecahydro-1H-7,11-methanocyclodeca[3,4]benzo[1,2-b]oxet-12-yl benzoate (7b). Compound **7b** was prepared as described for compound **5b** using compound **7a** (5.3 g, 5.0 mmol). The product was recovered as a white solid (2.5 g, 83% yield). ^{1}H NMR (δ ppm, DMSO-*d*6): 0.98 (s, 6H), 1.36 (s, 9H), 1.51 (s, 4H), 1.68 (s, 4H), 1.84 (m, 1H), 2.27 (m, 4H), 2.78 (m, 2H), 3.05 (m, 2H), 3.66 (m, 1H), 4.45 (s, 1H), 4.83-5.11 (br m, 7H), 5.18 (d, J = 7.5 Hz, 1H), 5.40 (d, J = 6.9 Hz, 1H), 5.78 (t, J = 9.0 Hz, 1H), 7.18 (t, J = 6.9 Hz, 1H), 7.35-7.46 (m, 5H), 7.63-7.76 (m, 3H), 7.92 (d, J = 9.3 Hz, 1H), 7.99 (d, J = 6.9 Hz, 2H). MS m/z calculated for $C_{48}H_{60}N_2O_{17}$, 936.39, found $[M+H]^+$, 937.4.

DTX-β-alanine-glycolate NDC (7c). Compound **7c** was prepared as described for compound **1c** using CDP copolymer (2.0 g, 0.41 mmol) in dry DMF (20 mL), **7b** (0.94 g, 0.91 mmol), DIEA (0.12 g, 0.91 mmol), EDC·HCl (0.17 g, 0.91 mmol), and NHS (0.11 g, 0.91 mmol). See Table 1 for DLS characterization, concentration, loading, and purity data.

(2aR,4S,4aS,6R,9S,11S,12S,12aR,12bS)-12b-Acetoxy-9-(((R)-12-((S)-((tert-butoxycarbonyl)amino)(phenyl)methyl)-1-(4-methoxyphenyl)-10-oxo-1,1-diphenyl-9,11-dioxa-5,6-dithia-2-azatridecan-13-oyl)oxy)-4,6,11-trihydroxy-4a,8,13,13-tetramethyl-5-oxo-2a,3,4,4a,5,6,9,10,11,12,12a,12b-dodecahydro-1H-7,11-methanocyclodeca[3,4]benzo[1,2-b]oxet-12-yl benzoate (8a). Compound **4** (3.6 g, 8.2 mmol) was dissolved in ACN and mixed with disuccinimidyl carbonate (2.6 g, 10 mmol). After 3 hours this mixture was transferred to a solution of DTX (6.2 g, 7.6 mmol) and DMAP (1.0 g, 8.4 mmol) in DCM (100 mL) and stirred at RT overnight. The reaction mixture was concentrated to a solid, re-dissolved in EtOAc (100 mL), washed with water (2 x 50 mL) and dried. The product was column-purified using 0-100% EtOAc:DCM to produce a white powder (4.1 g, 43 % yield). ^{1}H NMR (δ ppm, $CDCl_3$): 0.88 (s, 6H), 1.32 (s, 9H), 1.75 (s, 4H), 1.94 (s, 3H), 2.45 (m, 5H), 2.70 (t, J = 7.1 Hz, 2H), 2.80 (t, J = 6.2 Hz, 2H), 3.77 (s, 3H), 3.93 (d, J = 6.7 Hz, 1H), 4.28 (m, 6H), 4.96 (d, J = 7.6 Hz, 1H), 5.22 (s, 1H), 5.27 (s, 1H), 5.48 (m, 2H), 5.69 (d, J = 7.0 Hz, 1H), 6.28 (t, J = 9.4 Hz, 1H), 6.81 (d, J = 9.1 Hz, 2H), 7.15-7.62 (m, 22H), 8.11 (d, J = 8.3 Hz, 2H).

(2aR,4S,4aS,6R,9S,11S,12S,12aR,12bS)-12b-Acetoxy-9-(((2R,3S)-2-(((2-((2-aminoethyl)disulfanyl)ethoxy)carbonyl)oxy)-3-((tert-butoxycarbonyl)amino)-3-phenylpropanoyl)oxy)-4,6,11-trihydroxy-4a,8,13,13-tetramethyl-5-oxo-2a,3,4,4a,5,6,9,10,11,12,12a,12b-dodecahydro-1H-7,11-methanocyclodeca[3,4]benzo[1,2-b]oxet-12-yl benzoate (8b). Compound **8b** was prepared as described for compound **4b** using compound **8a** (13 g, 9.8 mmol). The product was recovered as a white solid (9.5 g, 85 % yield). ^{1}H NMR (δ ppm, DMSO-*d*6): 0.98 (s, 6H), 1.36 (s, 9H), 1.51 (s, 4H), 1.75 (s, 4H), 1.85 (m, 1H), 2.25 (m, 4H), 2.75 (m, 4H), 3.00 (t, J = 6.1 Hz, 2H), 3.64 (d, J = 7.2 Hz, 1H), 4.03 (m, 3H), 4.39 (m, 2H), 4.91 (d, J = 9.6 Hz, 1H), 5.04-5.11 (m, 3H),

5.40 (d, J = 6.9 Hz, 1H), 5.80 (t, J = 9.0 Hz, 1H), 7.18 (t, J = 6.9 Hz, 1H), 7.35-7.46 (m, 5H), 7.65-7.74 (m, 3H), 7.99 (d, J = 7.2 Hz, 2H). MS m/z calculated for $C_{48}H_{62}N_2O_{16}S_2$, 986.35, found $[M+H]^+$, 987.6.

DTX-disulfide NDC (8c). Compound **8c** was prepared as described for compound **1c** using CDP copolymer (1.0 g, 0.21 mmol) in dry DMF (10 mL), **8b** (0.54 g, 0.47 mmol), DIEA (0.061 g, 0.47 mmol), EDC·HCl (0.090 g, 0.47 mmol), and NHS (0.054 g, 0.47 mmol). See Table 1 for DLS characterization, concentration, loading, and purity data.

4.3.3. Syntheses of Gemcitabine NDCs

(2R,3R,5R)-5-(4-Amino-2-oxopyrimidin-1(2H)-yl)-4,4-difluoro-2-(hydroxymethyl)tetrahydrofuran-3-yl tert-butyl carbonate (9). Gemcitabine (1.2 g, 4.0 mmol) and Na_2CO_3 (2.1 g, 20 mmol) were dissolved in aq. dioxane. Di-*tert*-butyl dicarbonate (0.88 g, 4.0 mmol) was added and the mixture stirred for 2 days. The desired product was extracted with EtOAc and purified by column flash chromatography with a 0 -20 % DCM:acetone gradient. The product was isolated as white solid (850 mg, 59 % yield). ^{1}H NMR (δ ppm, acetone-*d*6): 1.49 (s, 9H), 3.97 (m, 2H), 4.20 (m, 1H), 5.23 (m, 1H), 5.98 (d, J = 7.4 Hz, 1H), 6.33 (t, J = 8.8 Hz, 1H), 6.77 (s, 1H), 7.78 (d, J = 6.0 Hz, 1H). MS m/z calculated for $C_{14}H_{19}F_2N_3O_6$, 363.12, found $[M+H]^+$, 364.3.

tert-Butyl-(1-((2R,4R,5R)-4-((tert-butoxycarbonyl)oxy)-3,3-difluoro-5-(hydroxymethyl)tetrahydrofuran-2-yl)-2-oxo-1,2-dihydropyrimidin-4-yl)carbamate (10). Compound **9** (0.36 g, 1.0 mmol), di-*tert*-butyl dicarbonate (2.2 g, 10 mmol) and dioxane (40 mL) were mixed, stirred for 2 days. The product was extracted with EtOAc and purified by column chromatography in 0 - 20 % DCM:acetone to give a white solid (0.30 g, 65 % yield). ^{1}H NMR (δ ppm, acetone-*d*6): 1.50 (s, 9H), 1.51 (s, 9H), 3.01 (m, 1H), 3.97 (m, 2H), 4.20 (m, 1H), 5.27 (m, 1H), 6.35 (t, J = 8.9 Hz, 1H), 7.63 (s, 1H), 7.92 (d, J = 6.0 Hz, 1H). MS m/z calculated for $C_{19}H_{22}F_2N_3O_8$, 463.18, found $[M+H]^+$, 464.1.

((2R,3R,5R)-5-(4-((tert-Butoxycarbonyl)amino)-2-oxopyrimidin-1(2H)-yl)-3-((tert-butoxycarbonyl)oxy)-4,4-difluorotetrahydrofuran-2-yl)methyl-(tert-butoxycarbonyl)glycinate (11a).

Compound **10** (0.76 g, 1.6 mmol), Boc-glycine (0.32 g, 1.8 mmol), EDC·HCl (0.68 g, 3.3 mmol), and DMAP (0.21 g, 1.8 mmol) were dissolved in DCM (20 mL) and stirred at RT overnight. The reaction was diluted with ethyl acetate (100 mL) and washed with water (2 x 50 mL) and brine (20 mL). The organic layer was removed and the product was purified by flash chromatography with 0 - 20% DCM:acetone (0.81 g, 80 % yield). ^{1}H NMR (δ ppm, acetone): 1.42 (s, 9H), 1.49 (s, 9H), 1.51 (s, 9H), 3.92 (m, 2H), 4.51 (m, 2H), 4.70 (dd, J = 12.0, 2.3 Hz, 1H), 5.34 (m, 1H), 6.41 (m, 2H), 7.33 (d, *J* = 7.7 Hz, 1H), 8.01 (d, *J* = 7.3 Hz, 1H), 9.18 (s, 1H).

((2R,3R,5R)-5-(4-Amino-2-oxopyrimidin-1(2H)-yl)-4,4-difluoro-3-hydroxytetrahydrofuran-2-yl)methyl glycinate (11b). Removal of the Boc groups was achieved by dissolving **11a** (0.70 g, 1.1 mmol) in TFA (50 % by volume in DCM). The solvents were removed and the product was lyophilized to a white powder (0.53 g, 90 % yield). ^{1}H NMR (δ ppm, acetone-*d*6): 4.27 (m, 2H), 4.60 (m, 3H), 4.95 (s, 1H), 6.15 (m, 1H), 6.39 (m, 1H), 8.00 (d, *J* = 7.3 Hz, 1H). MS m/z calculated for $C_{11}H_{14}F_2N_4O_5$, 320.09, found $[M+H]^+$, found 321.1

GEM-glycinate NDC (11c). Compound **11c** was prepared as described for compound **1c** using CDP copolymer (2.0 g, 0.41 mmol) in dry DMF (20 mL), **11b** (0.47 g, 0.91 mmol), EDC·HCl (0.17 g, 0.91 mmol), NHS (0.11 g, 0.91 mmol), and DIEA (0.12 g, 0.91 mmol). See Table 1 for DLS characterization, concentration, loading, and purity data.

((2R,3R,5R)-5-(4-((tert-Butoxycarbonyl)amino)-2-oxopyrimidin-1(2H)-yl)-3-((tert-butoxycarbonyl)oxy)-4,4-difluorotetrahydrofuran-2-yl)methyl-6-((tert-butoxycarbonyl)amino)hexanoate (12a). Compound **12a** was prepared as described for compound **11a** using compound **10** (1.3 g, 2.8 mmol), Boc-aminohexanoic acid (0.84 g, 3.6 mmol), EDC·HCl (0.69 g, 3.6 mmol), and DMAP (0.44 g, 3.6 mmol). The product was recovered as a white solid (1.6 g, 85% yield). ^{1}H NMR (δ ppm, acetone-*d*6): 1.39 (s, 9H), 1.50 (m, 22H), 1.66 (m, 2H), 2.43 (t, *J* = 7.3 Hz, 2H), 3.06 (q, *J* =

6.9 Hz, 2H), 4.50 (m, 3H), 5.34 (s, 1H), 5.89 (s, 1H), 6.36 (t, J = 8.7 Hz, 1H), 7.27 (d, J = 7.7 Hz, 1H), 7.99 (d, J = 7.7 Hz, 1H), 9.19 (s, 1H).

((2R,3R,5R)-5-(4-Amino-2-oxopyrimidin-1(2H)-yl)-4,4-difluoro-3-hydroxytetrahydrofuran-2-yl)methyl 6-aminohexanoate (12b). Compound **12b** was prepared as described for compound **11b** using compound **12a** (1.6 g, 2.4 mmol). The product was recovered as a white solid (1.1 g, 85 % yield). ^{1}HNMR (δ ppm, acetone-*d*6): 1.50 (m, 2H), 1.69 (m, 2H), 1.86 (m, 2H), 2.45 (m, 2H), 3.83 (t, J = 7.4 Hz, 2H), 4.28 (m, 1H), 4.45 (m, 3H), 6.22 (t, J = 7.6 Hz, 1H), 6.39 (d, J = 7.7 Hz, 1H), 7.95 (d, J = 8.2 Hz, 1H). MS m/z calculated for $C_{22}H_{22}F_2N_4O_5$, 376.16, found $[M+H]^+$,found 377.2.

GEM-hexanoate NDC (12c). Compound **12c** was prepared as described for compound **1c** using CDP copolymer (2.0 g, 0.41 mmol) in DMF (20 mL), **12b** (0.43 g, 0.91 mmol), EDC·HCl (0.17 g, 0.91 mmol), NHS (0.11 g, 0.91 mmol), and DIEA (0.12 g, 0.91 mmol). See Table 1 for DLS characterization, concentration, loading, and purity data.

2-((3-((tert-Butoxycarbonyl)amino)propanoyl)oxy)acetic acid (13). A 100-mL round-bottom flask equipped with a magnetic stirrer was charged with 3-((tert-butoxycarbonyl)amino)propanoic acid (1.0 g, 5.3 mmol), benzyl 2-bromoacetate (1.2 g, 5.3 mmol), acetone (20 mL), and K_2CO_3 (1.1 g, 7.9 mmol). The mixture was heated for 2 h at reflux. The mixture was cooled to ambient temperature and filtered. The filtrate was concentrated to a residue, dissolved in EtOAc (20 mL), and washed with water (2 × 20 mL). The organic layer was separated, dried over sodium sulfate, and filtered. The residue was purified to afford the desired product as a colorless oil (1.5 g, 84 % yield). ^{1}H NMR (δ ppm, $CDCl_3$): 1.44 (s, 9H), 2.63 (t, J = 6.0 Hz, 2H), 3.44 (m, 2H), 4.69 (s, 2H), 5.13 (br s, 1H), 5.21 (s, 2H), 7.36 (m, 5H). A 250-mL stainless steel reactor equipped with a magnetic stirrer was charged with 2-(benzyloxy)-2-oxoethyl 3-((tert-butoxycarbonyl)amino)propanoate (1.00 g, 2.96 mmol), PtO_2 (0.14 g, 0.60 mmol), THF (30 mL). The reactor was sealed and hydrogen gas was flushed through two times. After that, the reactor was pressurized with hydrogen up to 80 psi and stirred overnight. The mixture was filtered and the filtrate was concentrated

in vacuum to afford the desired product as colorless oil (0.71 g, 96 % yield). ^{1}H NMR (δ ppm, $CDCl_3$): 1.43 (s, 9H), 2.62 (t, J = 6 Hz, 2H), 3.46 (m, 2H), 4.68 (s, 2H), 5.30 (br s).

2-(((2R,3R,5R)-5-(4-((tert-Butoxycarbonyl)amino)-2-oxopyrimidin-1(2H)-yl)-3-((tert-butoxycarbonyl)oxy)-4,4-difluorotetrahydrofuran-2-yl)methoxy)-2-oxoethyl-3-((tert-butoxycarbonyl)amino)propanoate (13a). Compound **10** (0.76 g, 1.6 mmol) in DCM (20 mL) was mixed with **13** (0.43 g, 1.7 mmol), DCC (0.68 g, 3.3 mmol), and DMAP (4.0 mg, 0.030 mmol). The organic layer was washed with water (20 mL) and concentrated to dryness under reduced pressure. The product was purified by flash chromatography using a 0 – 100 % hexanes:EtOAc gradient (0.99 g, 87% yield). ^{1}HNMR (δ ppm, $CDCl_3$): 1.52 (s, 18H), 2.67 (m, 2H), 3.45 (t, J = 5.5 Hz, 2H), 4.37 (m, 2H), 4.69 (m, 3H), 5.09 (m, 1H), 5.11 (m, 1H), 6.42 (m, 1H), 7.33 (d, J = 7.5 Hz, 1H), 7.47 (br s, 1H), 7.68 (d, J = 7.5 Hz, 1H).

2-(((2R,3R,5R)-5-(4-Amino-2-oxopyrimidin-1(2H)-yl)-4,4-difluoro-3-hydroxytetrahydrofuran-2-yl)methoxy)-2-oxoethyl 3-aminopropanoate (13b). Compound **13b** was prepared as described for compound **11b** using compound **13a** (2.9 g, 4.1 mmol). The product was recovered as a white solid (1.8 g, 74 % yield). ^{1}HNMR (δ ppm, DMSO-*d*6): 2.77 (t, J = 7.0 Hz, 2H), 3.07 (m, 2H), 4.11 (m, 1H), 4.27 (m, 1H), 4.40 (m, 2H), 6.14 (m, 2H), 7.83 (d, J = 8.0 Hz, 1H), 7.91 (br s, 3H), 9.06 (br s, 1H), 9.39 (br s, 1H). MS m/z calculated for $C_{14}H_{14}F_2N_4O_7$, 392.32, found $[M+H]^+$, 393.3.

GEM-β-alanine-glycolate NDC (13c). Compound **13c** was prepared as described for compound **1c** using CDP copolymer (2.0 g, 0.41 mmol) in dry DMF (20 mL), **14b** (0.54 g, 0.91mmol), EDC·HCl (0.17 g, 0.91 mmol), NHS (0.11 g, 0.91 mmol), and DIEA (0.12 g, 0.91 mmol). See Table 1 for DLS characterization, concentration, loading, and purity data.

4.4. NDC Preparation for Testing

NDCs were prepared for testing by thawing the respective aqueous nanoparticle solutions and adding solid mannitol (1.25 wt equiv. per NDC) under stirring. The resulting solution was then diluted with water to the desired concentration and filtered through Millipore Steriflip 0.22-μm filter. Nanoparticle solutions were stored at -20 °C until further usage.

4.5. In Vitro Drug Release Studies

In vitro drug release samples were prepared by diluting a NDC stock solution (0.3 mL) with PBS (2.7 mL). Sample aliquots (150 μL) were then incubated at 37 ^{o}C, and for each time point (single data point for each time point) the sample was quenched with ACN (75 μL containing 0.1% formic acid). Samples were analyzed by HPLC for the concentration of released drug, CBTX, DTX, or GEM. During method development, the assay was run several times in different settings to understand each NDC system (*i.e.*, payload and linker) including confirmation of results by a second analyst. For each NDC series (i.e., same payload, different linkers) drug release was run for all linkers at the same time, to allow direct to direct comparison.

4.6. Pharmacokinetic (PK) Studies

This work was approved by the research site IACUC prior to initiation. For CBTX, male C57BL/6 mice (Taconic Farms, Germantown, NY; N = 3 per time point) were implanted subcutaneously with B16.F10 tumor cells. Implants were performed by subcutaneous injection of $5x10^6$ tumor cells suspended in a mixture of EMEM:Matrigel (1:1) in the flank. When mean tumor volumes reached 398 mm^3, mice were administered a single intravenous treatment of CBTX or the corresponding NDCs at the CBTX equivalent dose of 13.5 mg/kg. After dosing, blood was collected at the time-points 5, 15, and 30 min, then 2, 6, 24, 72, 120 and 168 hours from mice with B16.F10 xenografts. All mice were euthanized by CO_2 inhalation. Plasma was prepared, diluted 1:1 with 0.2% formic acid, and frozen at -20^{o}C until analyses. Xenografts with B16.F10 tumor cells were collected at 5, 15, and 30 min, then 2, 6, 24, 72, 120 and 168 hours post dose and stored frozen until analysis. Finally for GEM, male C57BL/6 mice (Taconic Farms, Germantown, NY) were administered a single intravenous treatment of GEM at a dose of 10 mg/kg for the parent drug and 10 mg/kg (GEM equivalent dose) for the corresponding NDCs. Blood was collected at 5, 15, and 30 min, then 1, 2, 6, 24, and 72 hours from the time of dosing. The mice were euthanized by cardiac puncture. Plasma was prepared, diluted 1:1 with 0.2% formic acid, and frozen at -20^{o}C until analyses.

The targeted covalent conjugation of the API drug to the CDP copolymer and the possibility to break this bond via focused chemical hydrolysis afforded us to determine both the total (conjugated + released) amount of drug and the released amount of drug in just 2 aliquots from the same plasma or tumor tissue sample. Sample preparation for standard free drug analysis was achieved by transferring diluted mouse plasma (50 μL) into a 96-well plate. Internal standard stock solution (300 μL) was added to the plasma, followed by vortexing, and centrifugation (1000xg for 10 min). Sample aliquots (200 μL) were then transferred to another 96-wells plate and the solvent evaporated under nitrogen flow. An ACN-water mixture (1:1, containing 0.1% formic acid, 60 μL) was added to each well, and each sample was analyzed by LC-MS/MS for free drug content. Plasma samples for total drug analysis were prepared by transferring diluted mouse plasma (50 μL) into a 96-well plate. Hydroxylamine (10 μL) was added to each plasma solution and the plate incubated overnight at 4^{o}C to release all drug from the NDC. Internal standard stock solution (300 μL) was added to the plasma, followed by vortex mixing, and centrifugation (1000xg for 10 min). Sample aliquots (200 μL) were then transferred to another 96-wells plate and the solvent evaporated under nitrogen flow. An ACN-water mixture (1:1, containing 0.1% formic acid, 60 μL) was added to each well, and each sample was analyzed by LC-MS/MS for total drug content.

One ml of phosphate buffer containing a protease inhibitor cocktail was added to weighed tumor samples and the tissue was homogenized using a hand-held rotating-blade homogenizer. Aliquots of the tissue homogenates were transferred to 96-well plates and sample preparation for total and released drug was performed in parallel to that for plasma samples.

4.7. Efficacy Studies

This work was approved by the research site IACUC prior to initiation. For the B16.F10 study, male C57BL/6 mice (N = 8) were implanted subcutaneously with B16.F10 tumor cells as described above for PK studies. CBTX and the corresponding NDCs were administered intravenously at the MTD of 24, 24 and 30 mg/kg, respectively, every 7 days for 2 treatments (qwx2), beginning when the mean tumor volume was

60 mm^3. For the UISO-BCA-1 xenograft tumor study, female ICR SCID mice (N = 8) were implanted subcutaneously with cells as described above. CBTX and the corresponding NDCs were administered intravenously at the respective MTDs every 7 days for 2 treatments (qwx2), beginning when the mean tumor volume was 170 mm^3. The vehicle control was 10% sucrose in TE buffer.

Statistical data analyses were conducted in Prism 7.04. The efficacy was analyzed by time-to-event method (survival method). For the B16.F10 study, the event for this comparison was defined as the tumor volume reaching 3000 mm^3. The Log-rank test showed there were statistically significant difference (p-value <0.0001) between four groups (Vehicle, CBTX, CBTX-GLY, and CBTX-Hex). There were statistically significant difference (p-value <0.0001) between 3 treated groups (CBTX, CBTX-GLY, and CBTX-Hex) but no significant difference (p-value 0.86) found between CBTX-GLY and CBTX-Hex. When animals were euthanized due to ethical reasons, the tumor volume data could not be analyzed using parametric methods such as t-test/ANOVA because of the informative dropout issue. However, those early time points that had complete data were analyzed using unequal variance t-tests and showed Vehicle separated from the treated group as early as day 14. For the UISO-BCA-1 xenograft tumor study, the event for this comparison was defined as the tumor volume reaching 1000 mm^3. The Log-rank test showed there were statistically significant difference (p-value <0.0001) between four groups (Vehicle, CBTX, CBTX-GLY, and CBTX-Hex). There were no statistically significant difference (p-value <0.32) found between 3 treated groups (CBTX, CBTX-GLY, and CBTX-Hex). When animals were euthanized due to ethical reasons, the tumor volume data could not be analyzed using parametric methods such as t-test/ANOVA because of the informative dropout issue. However, those early time points that had complete data were analyzed using unequal variance t-tests and showed Vehicle separated from the CBTX and CBTX-Gly as early as day 17 and separated from CBTX-Hex as early as day 23.

5. Ancillary Information.

Supporting Information

(1) HPLC traces of key NDC test compounds, (2) Representative ^{1}H NMR trace of CBTX-hexanoate-NH_2 **2b**, and (3) Molecular formula strings.

Corresponding Author

Chester A. Metcalf III, chet.metcalf@novartis.com

Acknowledgements

The authors thank the scientists and management teams of Cerulean and Novartis for their support of this work. This assistance was funded by Novartis, Cambridge, MA.

Abbreviations Used

CDP, β-Cyclodextrin-PEG; EPR, Enhanced Permeability and Retention Effect; NDC, Nanoparticle-Drug Conjugate

6. References

1. Shi, J.; Kantoff, P. W.; Wooster, R.; Farokhzad, O. C. Cancer nanomedicine: progress, challenges and opportunities. *Nature Rev. Cancer* **2017**, *17*, 20-37.

2. Dizon, D. S.; Krilov, L.; Cohen, E.; Gangadhar, T.; Ganz, P. A.; Hensing, T. A.; Hunger, S.; Krishnamurthi, S. S.; Lassman, A. B.; Markham, M. J.; Mayer, E.; Neuss, M.; Pal, S. K.; Richardson, L. C.; Schilsky, R.; Schwartz, G. K.; Spriggs, D. R.; Villalona-Calero, M. A.; Villani, G.; Masters, G. Clinical cancer advances 2016: annual report on progress against cancer from the American Society of Clinical Oncolog. *J Clin. Oncol.* **2016**, *34*, 987-1011.

3. Kong, M.; Park, H.; Cheng, X.; Chen, X. Spatial-temporal event adaptive characteristics of nanocarrier drug delivery in cancer therapy. *J. Control Release* **2013,** *172*, 281-291.

4. Maeda, H. Macromolecular therapeutics in cancer treatment: the EPR effect and beyond. *J. Control Release* **2012,** *164*, 138-144.

5. Mura, S.; Nicolas, J.; Couvreur, P. Stimuli-responsive nanocarriers for drug delivery. *Nature Mater.* **2013**, *12*, 991-1003.

6. Pérez-Herrero, E.; Fernández-Medarde, A. Advanced targeted therapies in cancer: drug nanocarriers, the future of chemotherapy. *Eur. J. Pharm. Biopharm.* **2015**, *93*, 52-79.

7. Ferrari, M. Frontiers in cancer nanomedicine: directing mass transport through biological barriers. *Trends Biotechnol.* **2010,** *28*, 181-188.

8. Spencer, D. S.; Puranik, A. S.; Peppas, N. A. Intelligent nanoparticles for advanced drug delivery in cancer treatment. *Curr. Opin. Chem. Eng.* **2015**, *7*, 84-92.

9. Wicki, A.; Witzigmann, D.; Balasubramanian, V.; Huwyler, J. Nanomedicine in cancer therapy: challenges, opportunities, and clinical applications. *J. Control Release* **2015**, *200*, 138-157.

10. Sawant, R. T., V. Multifunctional nanocarriers and intracellular drug delivery. *Current Opinion in Solid State and Materials Science* **2012,** *16*, 269-275.

11. Heidel, J. D.; Davis, M. E. Clinical developments in nanotechnology for cancer therapy. *Pharm. Res.* **2011,** *28*, 187-199.

12. Svenson, S. Clinical translation of nanomedicines. *Current Opinion in Solid State and Materials Science* **2012,** *16*, 287-294.

13. Schutz, C. A.; Juillerat-Jeanneret, L.; Mueller, H.; Lynch, I.; Riediker, M.; NanoImpactNet, C. Therapeutic nanoparticles in clinics and under clinical evaluation. *Nanomedicine (Lond.)* **2013,** *8*, 449-467.

14. Duncan, R.; Gaspar, R. Nanomedicine(s) under the microscope. *Mol. Pharm.* **2011,** *8*, 2101-2141.

15. Pham, E.; Birrer, M. J.; Eliasof, S.; Garmey, E. G.; Lazarus, D.; Lee, C. R.; Man, S.; Matulonis, U. A.; Peters, C. G.; Xu, P.; Krasner, C.; Kerbel, R. S. Translational impact of nanoparticle-drug conjugate CRLX101 with or without bevacizumab in advanced ovarian cancer. *Clin. Cancer Res.* **2015,** *21*, 808-818.

16. Sen, K.; Mandal, M. Second generation liposomal cancer therapeutics: transition from laboratory to clinic. *Int. J. Pharm.* **2013,** *448*, 28-43.

17. Jhaveri, A.; Deshpande, P.; Torchilin, V. P. Stimuli-sensitive nanopreparations for combination cancer therapy. *J. Control Release* **2014**, *190*, 352-370.

18. Al-Jamal, W. T.; Kostarelos, K. Liposomes: from a clinically established drug delivery system to a nanoparticle platform for theranostic nanomedicine. *Acc. Chem. Res.* **2011,** *44*, 1094-1104.

19. Barenholz, Y. Doxil(R)--the first FDA-approved nano-drug: lessons learned. *J. Control Release* **2012,** *160*, 117-134.

20. Nishiyama, N.; Matsumura, Y.; Kataoka, K. Development of polymeric micelles for targeting intractable cancers. *Cancer Sci.* **2016**, *107*, 867-874.

21. Sun, T.; Zhang, Y. S.; Pang, B.; Hyun, D. C.; Yang, M.; Xia, Y. Engineered nanoparticles for drug delivery in cancer therapy. *Angew. Chem. Int. Ed.* **2014**, *53*, 12320-12364.

22. Gaucher, G.; Marchessault, R. H.; Leroux, J. C. Polyester-based micelles and nanoparticles for the parenteral delivery of taxanes. *J. Control Release* **2010,** *143*, 2-12.

23. Gong, J.; Chen, M.; Zheng, Y.; Wang, S.; Wang, Y. Polymeric micelles drug delivery system in oncology. *J. Control Release* **2012,** *159*, 312-323.

24. Talelli, M. R., C.; Hennink, W.; Lammers, T. Polymeric micelles for cancer therapy: 3 C's to enhance efficacy. *Current Opinion in Solid State and Materials Science* **2012,** *16*, 302-309.

25. Suk, J. S.; Xu, Q.; Kim, N.; Hanes, J.; Ensign, L. M. PEGylation as a strategy for improving nanoparticle-based drug and gene delivery. Adv. *Drug Deliv. Rev.* **2016**, *99*, 28-51.

26. Fleige, E.; Quadir, M. A.; Haag, R. Stimuli-responsive polymeric nanocarriers for the controlled transport of active compounds: concepts and applications. *Adv. Drug Deliv. Rev.* **2012,** *64*, 866-884.

27. Morachis, J. M.; Mahmoud, E. A.; Almutairi, A. Physical and chemical strategies for therapeutic delivery by using polymeric nanoparticles. *Pharmacol. Rev.* **2012,** *64*, 505-519.

28. Desai, N. Challenges in development of nanoparticle-based therapeutics. *AAPS J.* **2012,** *14*, 282-295.

29. Pinkerton, N. M.; Grandeury, A.; Fisch, A.; Brozio, J.; Riebesehl, B. U.; Prud'homme, R. K. Formation of stable nanocarriers by *in situ* ion pairing during block-copolymer-directed rapid precipitation. *Mol. Pharm.* **2013,** *10*, 319-328.

30. Podobinski, J.; Ramstack, J. M.; Dickey, D. S. Methods and systems for generating nanoparticles. US patent 8,404,799, **2013**.

31. Lerch, S.; Dass, M.; Musyanovych, A.; Landfester, K.; Mailander, V. Polymeric nanoparticles of different sizes overcome the cell membrane barrier. *Eur. J. Pharm. Biopharm.* **2013,** *84*, 265-274.

32. Longmire, M. R.; Ogawa, M.; Choyke, P. L.; Kobayashi, H. Biologically optimized nanosized molecules and particles: more than just size. *Bioconjug. Chem.* **2011,** *22*, 993-1000.

33. Shah, N. B.; Vercellotti, G. M.; White, J. G.; Fegan, A.; Wagner, C. R.; Bischof, J. C. Blood-nanoparticle interactions and *in vivo* biodistribution: impact of surface PEG and ligand properties. *Mol. Pharm.* **2012,** *9*, 2146-2155.

34. Gindy, M. E.; Ji, S.; Hoye, T. R.; Panagiotopoulos, A. Z.; Prud'homme, R. K. Preparation of poly(ethylene glycol) protected nanoparticles with variable bioconjugate ligand density. *Biomacromolecules* **2008,** *9*, 2705-2711.

35. Perry, J. L.; Reuter, K. G.; Kai, M. P.; Herlihy, K. P.; Jones, S. W.; Luft, J. C.; Napier, M.; Bear, J. E.; DeSimone, J. M. PEGylated PRINT nanoparticles: the impact of PEG density on protein binding, macrophage association, biodistribution, and pharmacokinetics. *Nano. Lett.* **2012,** *12*, 5304-5310.

36. Walkey, C. D.; Olsen, J. B.; Guo, H.; Emili, A.; Chan, W. C. Nanoparticle size and surface chemistry determine serum protein adsorption and macrophage uptake. *J. Am. Chem. Soc.* **2012,** *134*, 2139-2147.

37. Ashton, S.; Song, Y. H.; Nolan, J.; Cadogan, E.; Murray, J.; Odedra, R.; Foster, J.; Hall, P. A.; Low, S.; Taylor, P.; Ellston, R.; Polanska, U. M.; Wilson, J.; Howes, C.; Smith, A.; Goodwin, R. J.; Swales, J. G.; Strittmatter, N.; Takats, Z.; Nilsson, A.; Andren, P.; Trueman, D.; Walker, M.; Reimer, C. L.; Troiano, G.; Parsons, D.; De Witt, D.; Ashford, M.; Hrkach, J.; Zale, S.; Jewsbury, P. J.; Barry, S. T. Aurora kinase

inhibitor nanoparticles target tumors with favorable therapeutic index *in vivo*. *Sci. Transl. Med.* **2016,** *8*, 325ra17.

38. a) Hrkach, J.; Von Hoff, D.; Ali, M. M.; Andrianova, E.; Auer, J.; Campbell, T.; De Witt, D.; Figa, M.; Figueiredo, M.; Horhota, A.; Low, S.; McDonnell, K.; Peeke, E.; Retnarajan, B.; Sabnis, A.; Schnipper, E.; Song, J. J.; Song, Y. H.; Summa, J.; Tompsett, D.; Troiano, G.; Van Geen Hoven, T.; Wright, J.; LoRusso, P.; Kantoff, P. W.; Bander, N. H.; Sweeney, C.; Farokhzad, O. C.; Langer, R.; Zale, S. Preclinical development and clinical translation of a PSMA-targeted docetaxel nanoparticle with a differentiated pharmacological profile. *Sci. Transl. Med.* **2012**, *4*, 128ra39; b) Gong, C.; Xie, Y.; Wu, Q.; Wang, Y.; Deng, S.; Xiong, D.; Liu, L.; Xiang, M.; Qian, Z.; Wei, Y. Improving antitumor activity with polymeric micelles entrapping paclitaxel in pulmonary carcinoma. *Nanoscale* **2012**, *4*, 6004-6017; c) Vasanti, S.; Preeti, S. Paclitaxel nanoparticles - an approach to improve the bioavailability. *Inter. J. of Pharm. Sci. Rev. and Res.* **2014**, *27*, 200-208; d) Guo, Y.; Niu, B.; Song, Q.; Zhao, Y.; Bao, Y.; Tan, S.; Si, L.; Zhang, Z. RGD-decorated redox-responsive D-α-tocopherol polyethylene glycol succinate-poly(lactide) nanoparticles for targeted drug delivery. *J. of Mat. Chem. B: Mat. for Biol. and Med.* **2016**, 4, 2338-2350.

39. a) Cheng, J; Khin, K. T.; Jensen, G. S.; Liu, A.; Davis, M. E. Synthesis of linear, β-cyclodextrin-based polymers and their camptothecin conjugates. *Bioconjugate Chem.* **2003**, *14*, 1007-1017; b) Numbenjapon, T.; Wang, J.; Colcher, D.; Schluep, T.; Davis, M. E.; Duringer, J.; Kretzner, L.; Yen, Y.; Forman, S. J.; Raubitschek, A. Preclinical results of camptothecin-polymer conjugate (IT-101) in multiple human lymphoma xenograft models. *Clin. Cancer Res.* **2009,** *15*, 4365-4373.

40. Svenson, S.; Wolfgang, M.; Hwang, J.; Ryan, J.; Eliasof, S. Preclinical to clinical development of the novel camptothecin nanopharmaceutical CRLX101. *J. Control Release* **2011,** *153*, 49-55.

41. Eliasof, S.; Lazarus, D.; Peters, C. G.; Case, R. I.; Cole, R. O.; Hwang, J.; Schluep, T.; Chao, J.; Lin, J.; Yen, Y.; Han, H.; Wiley, D. T.; Zuckerman, J. E.; Davis, M. E. Correlating preclinical animal studies and human clinical trials of a multifunctional, polymeric nanoparticle. *Proc. Natl. Acad. Sci. U S A* **2013,** *110*, 15127-15132.

42. Maeda, H. Tumor-selective delivery of macromolecular drugs via the EPR effect: background and future prospects. *Bioconjug. Chem.* **2010,** *21*, 797-802.

43. Maeda, H. Vascular permeability in cancer and infection as related to macromolecular drug delivery, with emphasis on the EPR effect for tumor-selective drug targeting. *Proc. Jpn. Acad. Ser. B Phys. Biol. Sci.* **2012,** *88*, 53-71.

44. Li, Y.; Wang, J.; Wientjes, M. G.; Au, J. L. Delivery of nanomedicines to extracellular and intracellular compartments of a solid tumor. *Adv. Drug. Deliv. Rev.* **2012,** *64*, 29-39.

45. Fredenberg, S.; Wahlgren, M.; Reslow, M.; Axelsson, A. The mechanisms of drug release in poly(lactic-co-glycolic acid)-based drug delivery systems--a review. *Int. J. Pharm.* **2011,** *415*, 34-52.

46. Ponta, A.; Bae, Y. PEG-poly(amino acid) block copolymer micelles for tunable drug release. *Pharm. Res.* **2010,** *27*, 2330-2342.

47. Modi, S.; Anderson, B. D. Determination of drug release kinetics from nanoparticles: overcoming pitfalls of the dynamic dialysis method. *Mol. Pharm.* **2013,** *10*, 3076-3089.

48. Gu, F.; Zhang, L.; Teply, B. A.; Mann, N.; Wang, A.; Radovic-Moreno, A. F.; Langer, R.; Farokhzad, O. C. Precise engineering of targeted nanoparticles by using self-assembled biointegrated block copolymers. *Proc. Natl. Acad. Sci. U S A* **2008,** *105*, 2586-2591.

49. Chan, J. M.; Zhang, L.; Yuet, K. P.; Liao, G.; Rhee, J. W.; Langer, R.; Farokhzad, O. C. PLGA-lecithin-PEG core-shell nanoparticles for controlled drug delivery. *Biomaterials* **2009,** *30*, 1627-1634.

50. Larson, N.; Ghandehari, H. Polymeric conjugates for drug delivery. *Chem. Mater.* **2012,** *24*, 840-853.

51. Sinha, R.; Kim, G. J.; Nie, S.; Shin, D. M. Nanotechnology in cancer therapeutics: bioconjugated nanoparticles for drug delivery. *Mol. Cancer Ther.* **2006,** *5*, 1909-1917.

52. Santi, D. V.; Schneider, E. L.; Reid, R.; Robinson, L.; Ashley, G. W. Predictable and tunable half-life extension of therapeutic agents by controlled chemical release from macromolecular conjugates. *Proc. Natl. Acad. Sci. U S A* **2012,** *109*, 6211-6216.

53. Zhao, H.; Rubio, B.; Sapra, P.; Wu, D.; Reddy, P.; Sai, P.; Martinez, A.; Gao, Y.; Lozanguiez, Y.; Longley, C.; Greenberger, L. M.; Horak, I. D. Novel prodrugs of SN38 using multiarm poly(ethylene glycol) linkers. *Bioconjug. Chem.* **2008,** *19*, 849-859.

54. Tong, R.; Cheng, J. Drug-initiated, controlled ring-opening polymerization for the synthesis of polymer-drug conjugates. *Macromolecules* **2012,** *45*, 2225-2232.

55. Weiss, G. J.; Chao, J.; Neidhart, J. D.; Ramanathan, R. K.; Bassett, D.; Neidhart, J. A.; Choi, C. H.; Chow, W.; Chung, V.; Forman, S. J.; Garmey, E.; Hwang, J.; Kalinoski, D. L.; Koczywas, M.; Longmate, J.; Melton, R. J.; Morgan, R.; Oliver, J.; Peterkin, J. J.; Ryan, J. L.; Schluep, T.; Synold, T. W.; Twardowski, P.; Davis, M. E.; Yen, Y. First-in-human phase 1/2a trial of CRLX101, a cyclodextrin-containing polymer-camptothecin nanopharmaceutical in patients with advanced solid tumor malignancies. *Invest. New Drugs* **2013,** *31*, 986-1000.

56. Khorsand, B.; Lapointe, G.; Brett, C.; Oh, J. K. Intracellular drug delivery nanocarriers of glutathione-responsive degradable block copolymers having pendant disulfide linkages. *Biomacromolecules* **2013,** *14*, 2103-2111.

57. Vrignaud, P.; Semiond, D.; Lejeune, P.; Bouchard, H.; Calvet, L.; Combeau, C.; Riou, J. F.; Commercon, A.; Lavelle, F.; Bissery, M. C. Preclinical antitumor activity of cabazitaxel, a semisynthetic taxane active in taxane-resistant tumors. *Clin. Cancer Res.* **2013,** *19*, 2973-2983.

58. Wilhelm, S.; Tavares, A. J.; Dai, Q.; Ohta, S.; Audet, J.; Dvorak, H. F.; Chan, W. C. W. Analysis of nanoparticle delivery to tumours. *Nat. Rev. Mater.* **2016,** *14*, 1-12.

59. Madden, A. J.; Rawal, S.; Sandison, K.; Schell, R.; Schorzman, A.; Deal, A.; Feng, L.; Ma, P.; Mumper, R.; DeSimone, J.; Zamboni, W. C. Evaluation of the efficiency of tumor and tissue delivery of carrier-mediated agents (CMA) and small molecule (SM) agents in mice using a novel pharmacokinetic (PK) metric: relative distribution index over time (RDI-OT). *J. Nanopart. Res.* **2014,** *2662*, 1-16.

60. http://pi.lilly.com/us/gemzar.pdf (accessed May 15, 2019).

61. Peters, C. G.; Lazarus, D.; Brown, D.; Zhang, N.; Case, R.; Rohde, E.; Eliasof, S.; Jayaraman, L. Selective Tumor Localization of CRLX101, an Investigational Novel Nanoparticle-drug Conjugate. *AACR-*

NCI-EORTC International Conference on Molecular Targets and Cancer Therapeutics, Boston, MA, United States, Nov 5-9, 2015, Abstract# B37.

62. Clark, A. J.; Wiley, D. T.; Zuckerman, J. E.; Webster, P.; Chao, J.; Lin, J.; Yen, Y.; Davis, M. E. CRLX101 nanoparticles localize in human tumors and not in adjacent, nonneoplastic tissue after intravenous dosing. *Proc. Natl. Acad. Sci. U S A* **2016,** *113*, 3850-3854.

63. a) Metcalf III, C. A.; Brown, D.; Hwang, J.; Kabir, S.; Lazarus, D.; Shum, P.; Tripathi, S.; Eliasof, S. In Vitro and In Vivo Studies Demonstrating Sustained Drug Release for Multiple Anticancer Payloads and Improved Anticancer Effects of a Cabazitaxel β-Cyclodextrin-PEG Copolymer-Based Nanoparticle-Drug Conjugate (NDC). *AACR-NCI-EORTC International Conference on Molecular Targets and Cancer Therapeutics, Boston, MA, Untited States, Nov 5-9, 2015,* Abstract# B176; b) Metcalf III, C. A.; van der Poll, D.; Zhao, L.; Halo, T.; Lazarus, D.; Stockmann, A.; Peters, C.; Brown, D.; Case, R. I.; Rohde, E.; Jayaraman, L.; Wang, H.; Crowell, T.; Senderowicz, A.; Eliasof, S. Significant Improvements in Therapeutic Index for Conjugated Payloads Using a Nanoparticle-Drug Conjugate (NDC) Platform to Provide Sustained Drug Release and Potentially Improved Anticancer Effects. *AACR Special Conference on Engineering and Physical Sciences in Oncology, Boston, MA, United States, June 25-28, 2016*, Abstract# B43.

7. Table of Contents Graphic